

# Proliferation and prevention of self-loops in ensembles of interacting binary elements

Paul Baconnier,<sup>1</sup> Margot H. Teunisse,<sup>1,2</sup> and Martin van Hecke<sup>1,2</sup>

<sup>1</sup>*AMOLF, 1098 XG Amsterdam, The Netherlands.*

<sup>2</sup>*Huygens-Kamerlingh Onnes Laboratory, Leiden University, 2300 RA Leiden, The Netherlands.*

Models based on spins or hysterons with appropriately chosen interactions can capture advanced memory effects in complex materials, such as transients in repeatedly compressed crumpled sheets or sequential computing in driven metamaterials. However, unphysical self-loops dominate the response when interactions are chosen randomly, undermining statistical approaches. Here, we uncover the origin of self-loop proliferation in randomly coupled models. We introduce the weakly asymmetric ensemble to suppress self-loops and then develop interaction ensembles that strictly eliminate them. Finally, we use these ensembles to explore the statistics of large systems. Our work highlights the subtle role of interaction symmetries and paves the way for statistical studies of the sequential response and memory effects in complex, multistable materials.

Sequences of transitions between metastable states govern the hysteresis [1], memory [2–9], emergent computing [10–12], sequential shape-morphing [13, 14], and adaptive behavior [15–17] of driven dissipative materials, such as crumpled sheets, disordered media, and metamaterials [9]. As these states often consist of local, binary elements, with or without hysteresis, the response can be described by models of interacting hysterons or binary spins at zero-temperature (Fig. 1a). While models without interactions are well understood [1, 18–20], interactions are crucial for capturing complex responses such as avalanches, transients, and multiperiodic cycles [5, 21]. In the rare cases that interactions can be measured [7, 10] or modeled [12, 22–26], they enable accurate predictions of the systems response and memory effects [5, 8, 10, 12, 26–28]. However, often the detailed interactions are unknown, and our goal is to understand classes of system through statistical studies of ensembles of interaction coefficients [4, 5, 21, 29–31].

Here we uncover that *random* asymmetric interactions inevitably lead to self-loops that overwhelm the response in large systems. Self-loops are avalanches that get trapped in a repeating sequence of states which never settles (Fig. 1b) [21, 32–35]. Such sustained loops are unphysical for slowly driven dissipative systems.

We stress that hysterons are strongly nonlinear, so that the Maxwell-Betti reciprocity relations no longer apply [36], and dissipation does not imply symmetry. This is in contrast to interacting *spins*, where symmetric interactions produce transitions that lower an energy and are thus free of self-loops [34, 37], while non-symmetric interactions can be associated with energy input which drives oscillations: self-loops [32–35, 38–42]. For hysterons, the asymmetry of the interaction matrix, where  $c_{ij}$  represents how hysteron  $i$ 's flipping threshold  $H_i$  is influenced by hysteron  $j$ , arises from differences in hysteron strength. For example, in a crumpled sheet, flipping a hysteron associated with a small ridge ( $i$ ) weakly affects a larger ridge ( $j$ ), while flipping hysteron  $j$  more strongly impacts  $i$ :  $|c_{ij}| < |c_{ji}|$  (Fig. 1c). Indeed, when measured or modeled, hysteron interactions are asymmetric [10, 12, 26], and asymmetry is crucial to capture observed memory effects [5]. We thus face a conundrum: while asymmetric interactions are necessary, random asymmetry leads to

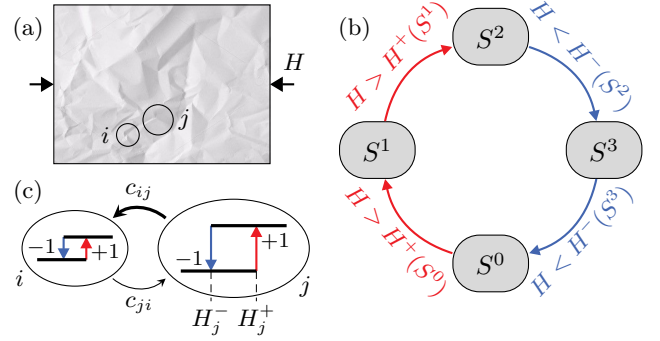


FIG. 1: Self-loops in driven multistable systems. (a) Schematic of a crumpled sheet where local ridges act as hysterons [7]. (b) Partial transition graph. The states ( $S^0, S^1, \dots$ ) undergo transitions when the driving  $H$  crosses the indicated switching fields (up: red, down: blue). If the system starts in state  $S^0$  and  $H$  is increased above the switching field  $H^+(S^0)$ , this causes the self-loop  $S^0 \rightarrow S^1 \rightarrow S^2 \rightarrow S^3 \rightarrow S^0 \rightarrow \dots$  when the switching fields satisfy  $H^+(S^1) < H^+(S^0)$ ,  $H^-(S^2) > H^+(S^0)$  and  $H^-(S^3) > H^+(S^0)$  (Supplemental Material). (c) Variations in hysteron strength lead to asymmetric interactions ( $|c_{ij}| > |c_{ji}|$ ).

self-loops inconsistent with dissipative behavior.

Here we uncover the mechanisms that produce self-loops. We first show that the absence of self-loops for symmetric interactions can be understood from the lowering of a pseudo energy. We then explore self-loops for asymmetric interactions and show that their probability asymptotes to one in large systems. We explore strict conditions associated with specific self-loops, derive precise criteria for short self-loops, and introduce weak asymmetry as a simple, lenient approach to suppress self-loops. We then present several strict ensembles that are completely free of self-loops. Finally, we explore the statistical properties of avalanches and the response to cyclic driving in large systems. Our work opens the route towards statistical studies of the sequential response of dissipative materials.

*Model.*— We consider  $N$  binary elements,  $s_i = \pm 1$ , which form collective states  $S = (s_1, s_2, \dots)$ . The system is driven by a global field  $H$ , and the stability range of each element  $i$  in state  $S$  is given by switching fields

$H_i^\pm(S)$ . For pairwise interactions:

$$H_i^\pm(S) = h_i^\pm - \sum_{j \neq i} c_{ij} s_j, \quad (1)$$

where  $h_i^\pm$  are the bare switching fields of element  $i$ . To model spins, we take  $h_i^+ = h_i^-$ , whereas for hysterons,  $h_i^+ > h_i^-$  [1, 19, 20]. The matrix  $c_{ij}$ , with  $c_{ii} = 0$ , encodes cooperative ( $c_{ij} > 0$ ) or frustrated ( $c_{ij} < 0$ ) interactions that may be asymmetric ( $c_{ij} \neq c_{ji}$ ) [5, 12, 26, 28].

In this model, each state  $S$  has a range of stability, encoded in state switching fields  $H^\pm(S)$  which follow from the extrema of  $H_i^\pm(S)$ :  $H^+(S) := \min_{i^-}(H_i^+(S))$  and  $H^-(S) := \max_{i^+}(H_i^-(S))$ , where  $i^\pm$  are the indices where  $s_i = \pm 1$ . When the system is in state  $S^0$  and  $H$  is increased above  $H^+(S^0)$  or decreased below  $H^-(S^0)$ , state  $S^0$  loses stability and its unstable hysteron flips. Depending on  $n_u$ , the number of unstable hysterons in the resulting state  $S^1$ , three different scenarios arise. When  $n_u = 0$ , state  $S^1$  is stable; when  $n_u = 1$ , state  $S^1$  is unstable and its unstable hysteron flips; when  $n_u > 1$ , multiple hysterons are unstable. The latter case, which is abundant in large systems (Supplemental Material), leads to a race condition, and requires a dynamical rule to specify the next step in the transition [10, 12, 21, 28, 31]. Importantly, in the remainder, we only flip the most unstable element [5]; this rule is physically plausible and corresponds to the zero-temperature limit of the Glauber dynamics [43, 44] (for other rules, which can have a drastic impact, see Supplemental Material).

*Hysterons with symmetric interactions.*— Although hysteron interactions are not expected to be symmetric, numerical sampling reveals that symmetric interactions consistently avoid self-loops. To rigorously demonstrate this, we constructed the pseudo-energy  $V(S)$ , which decreases with each flipping event (see Appendix A):

$$V(S) = - \sum_{i^-} \left[ s_i(H - h_i^+) + \frac{1}{2} \sum_{j \neq i} s_i s_j c_{ij} \right] - \sum_{i^+} \left[ s_i(H - h_i^-) + \frac{1}{2} \sum_{j \neq i} s_i s_j c_{ij} \right], \quad (2)$$

guaranteeing the absence of self-loops.

*Random asymmetric coupling: gaps and self-loops.*— We now exploit random interactions, where  $c_{ij}$  and  $c_{ji}$  are sampled independently. We uncover two related scenarios where interactions lead to self-loops. Suppose the system is in state  $S$  which goes unstable when the driving reaches the value  $H^c$ . In the first scenario, the ensuing sequence of transitions never reaches a stable state and the system gets trapped in a self-loop, despite the presence of other stable states at  $H = H^c$ . In the second scenario,  $H^c$  lies in a *gap*, a range of  $H$  where no state is stable, and the system then necessarily gets trapped in a self-loop. To investigate the statistics of gaps and self-loops, we sample the model using an event-driven algorithm [5]. We consider collections of hysterons with thresholds in a

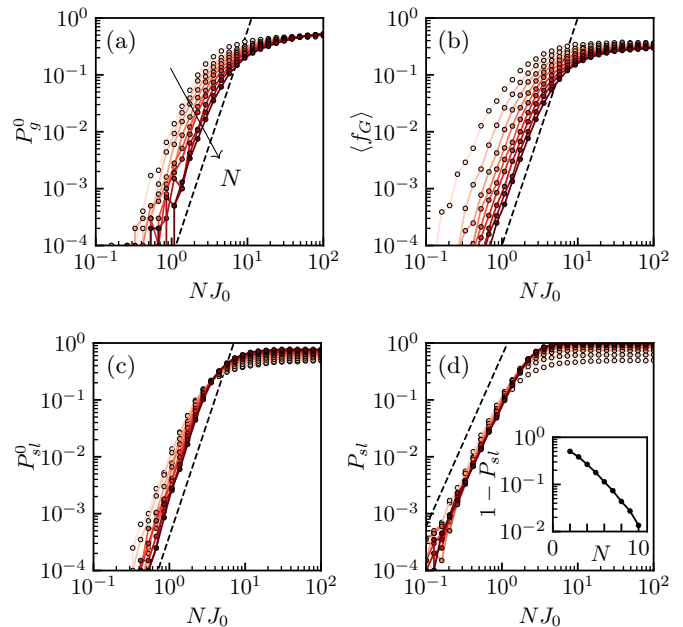


FIG. 2: Statistical measures for gaps and self-loops scale when plotted as function of  $NJ_0$  ( $10^5$  samples; color from light to dark as  $N$  increases from 2 to 10). (a) Probability  $P_g^0$  of finding a gap at  $H = 0$  (dashed line indicates slope 4). (b) Averaged fraction of gaps  $f_G$ , where  $f_G$  is defined as the ratio of the size of intervals where no stable states exist divided by  $[H^+(-\dots-), H^-(+\dots+)]$  (dashed line indicates slope 4). (c) Probability  $P_{sl}^0$  of finding at least one self-loops at  $H = 0$  (dashed line indicates slope 4). (d) Probability  $P_{sl}$  of finding at least one self-loop for any value of  $H$  (dashed line indicates slope 3). Inset: The probability to be self-loop free,  $1 - P_{sl}$ , decays to zero exponentially with  $N$  for large couplings ( $NJ_0 = 10^2$ ).

compact range [5, 8, 30], and for the bare switching fields, we flatly sample the midpoints  $h_i^c = (h_i^+ + h_i^-)/2$  from the interval  $[-1, 1]$  and the interaction coefficients  $c_{ij}$  from  $[-J_0, J_0]$ . Unless noted otherwise, we flatly sample the spans  $\sigma_i = h_i^+ - h_i^-$  from  $[0, 0.5]$ .

We find that the probability  $P_g^0$  of a gap, meaning the absence of a stable state at  $H = 0$ , and the fraction of gaps  $f_G$ , both increase as power laws when  $NJ_0 \ll 1$  (Figs. S3a-b). For  $NJ_0 \gg 1$ , they saturate at significant values, and the probability that states have a finite stability range decreases exponentially with  $N$  (Supplemental Material). To understand the emergence of gaps, consider the process of finding a stable state at a given driving field  $H$ . Each isolated element has one stable phase — two in the hysteretic range — for any value of  $H$ . Hence, in the absence of interactions, stable states are composed by combining stable elements. Interactions make each element's switching fields depend on the collective state, effectively randomizing stability ranges and creating gaps. As  $N$  increases, stable states become rare, making transitions harder to sample randomly.

Gaps imply self-loops, but self-loops can also occur without gaps: the probability of a self-loop occurring for a random state at  $H = 0$ ,  $P_{sl}^0$ , is larger than the corresponding gap probability  $P_g^0$  (Fig. S3c and Supplemental

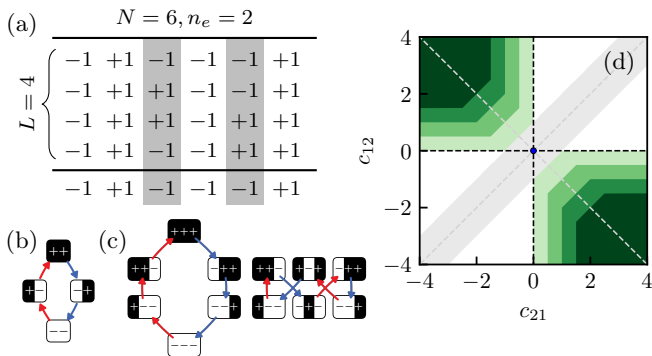


FIG. 3: (a) Example of the states in a self-loop ( $N = 6, L = 4, n_e = 2$ ). (b) The only fundamental  $L = 4$  self-loop (up/down transitions: red/blue arrows). (c) Two out of six possible  $L = 6$  fundamental self-loops — these are the only ones realizable with WA interactions (see Table I). (d) Location of  $L = 4$  self-loops for  $N = 2$  hysterons, where we fix  $\Delta h^c = 1$  and vary the minimal span  $\sigma$  from 0 to 3 by steps of 1 (light to dark green).

Material). Similarly, we calculated the probability of observing a self-loop at any value of  $H, P_{sl}$ , by starting from every stable state, in/decreasing  $H$ , and checking whether the ensuing transition yields a self-loop. We find that  $P_{sl}$  exceeds the corresponding fraction of gaps, and approaches one in large, strongly coupled systems (Fig. S3d; Supplemental Material). This dominance of self-loops is robust; hysterons with fixed spans  $\sigma_i = 0.5$  and binary spins where  $\sigma_i = 0$  also have  $P_{sl} \rightarrow 1$  (Supplemental Material) [32–35]. Hence, self-loops, incompatible with the dissipative systems we aim to model, are unavoidable for random interactions, and for large systems completely overwhelm the response.

*Proliferation of self-loops.*— Each self-loop is associated with a set of linear inequalities of  $(h_i^\pm, c_{ij})$ , and occurs in a polytope in parameter space [5, 21, 30, 31]. By identifying all potential self-loops, one could, in principle, determine all corresponding polytopes; the complement of their union is then free of self-loops. However, the number of self-loops grows rapidly with  $N$ .

We characterize each self-loop by its length  $L$  and by the  $n_e \leq N$  elements that are involved (Fig. S9a). We focus on *fundamental* loops, which are defined as the unique loops that involve all elements ( $n_e = N$ ) up to permutations (i.e., the self-loop  $(--)\rightarrow(-+)\rightarrow(++)\rightarrow(+--)\rightarrow\dots$  is equivalent to the loop in Fig. S9b). We determine the potential number of loops’ structures,  $M(n_e, L)$ , from the combinatorics of flip sequences, and calculate the number of realizable loops with pairwise interactions,  $M_R(n_e, L)$  (Supplemental Material). Both grow rapidly with  $n_e$  and  $L$  (Table I). In particular, for the shortest fundamental loops,  $M(n_e, L = 2n_e)$  grows as 1, 6, 56, 796, ... for  $n_e = 2, 3, 4, 5, \dots$  (Figs. S9-b and c for  $n_e = 2, 3$ ), and our data suggests that each of these is realizable. The number of actual self-loops and polytopes grows even faster with  $N$ . Introducing  $n_e$  elements into a larger group of  $N$  elements, and including permutations, maps each fundamental loop to a significantly larger number of actual loops and polytopes, fueling a

$L/n_e$	2	3	4	5
4	1/1/0	–	–	–
6	–	6/6/2	–	–
8	–	2/0/0	56/56/24	–
10	–	–	176/114/4	796/796/376
12	–	–	420/145/1	9028/x/x
14	–	–	448/48/0	76640/x/x
16	–	–	112/4/0	535584/x/x

Table I: Numbers of fundamental self-loops of size  $L$  involving  $n_e$  elements. Note that  $4 \leq L \leq 2^N$  and  $\log_2 L \leq n_e \leq L/2$ , as each element undergoes an even number of flips; loops with  $n_e$  elements can visit at most  $2^{n_e}$  states; and self-loops of size 2 are excluded by  $h_i^+ \geq h_i^-$  (Supplemental Material). The numbers in each box represents  $M(n_e, L)$ ,  $M_R(n_e, L)$ , and  $M_W(n_e, L)$ , respectively. Note that the number of longest fundamental loops,  $M(n_e, L = 2^{n_e})$ , are given by the number of directed Hamiltonian cycles in the binary  $n_e$ -cube (1, 2, 112, 15109096, ... for  $n_e = 2, 3, 4, 5, \dots$ ) [45, 46].

further combinatorial explosion.

*Lenient and strict strategies.*— The proliferation of the number, length, and complexity of self-loops for large  $N$ , makes deriving explicit and sharp conditions that identify all self-loops unfeasible. We thus first introduce a lenient strategy that fully eliminates the shortest self-loops and suppresses—though not completely eliminates—longer ones. We then define strict ensembles that entirely eliminate self-loops of any length but are overly limiting.

*Lenient strategy: weak asymmetry.*— Short ( $L = 4$ ) loops are sufficiently simple that we can derive their polytope conditions easily. First, for the simplest case of  $L = 4$  self-loops for two spins, we find that a gap of size  $|\Delta c| - |\Delta h^c|$  opens up when  $c_{12}c_{21} < 0$  and  $|\Delta c| > |\Delta h^c|$ , where  $\Delta c := c_{12} - c_{21}$  and  $\Delta h^c := h_2^c - h_1^c$ . These conditions turn out to be sufficient and necessary. For two hysterons, the upper bound of the spans  $\sigma_i$  is crucial: if it is zero, the same conditions apply, but if it is positive, there is a larger range in parameter space that is guaranteed to be free of  $L = 4$  self-loops (Fig. S9d). Finally, we can extend these conditions to arbitrary  $N$ ; as for  $L = 4$  self-loops only two elements  $i$  and  $j$  are involved, we can prevent short self-loops by requiring  $c_{ij}c_{ji} \geq 0$  for all  $(i, j)$  (For details, Supplemental Material).

We thus introduce the notion of weak asymmetry (WA):  $c_{ij}c_{ji} > 0$  for all  $(i, j)$ . This eliminates  $L = 4$  self-loops, and suppresses the number of longer self-loops (Table I, and Supplemental Material). Statistical sampling reveals that WA is an effective strategy to suppress self-loops. In particular,  $P_{sl}^0 \rightarrow 0$  for large  $N$ , allowing to sample individual transitions, although  $P_{sl}$  slowly grows with  $N$ : the combinatorial possibilities of finding a self-loop dominates in large systems. Nevertheless, for intermediate  $N$ , WA strongly suppresses self-loops, e.g.,  $P_{sl} \approx 14\%$  for large couplings and  $N = 10$ . Hence, WA strictly prohibits short self-loops and suppresses longer

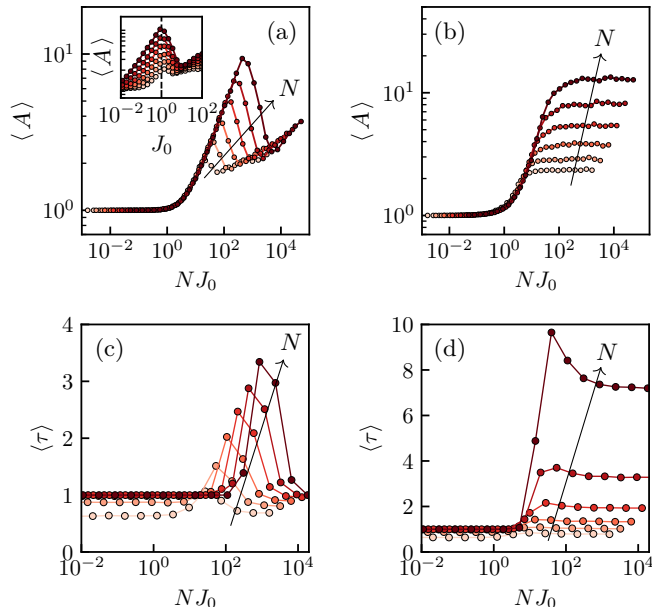


FIG. 4: Simulations of large systems of coupled hysterons in the constant-columns (left) and symmetric (right) ensembles ( $N = 16, 32, \dots, 512$  for increasingly dark colors). (a-b) Ensemble averaged avalanche size  $\langle A \rangle$ . To determine these, we initialize the system at a stable state  $S^0$  at  $H = 0$ , increase  $H$ , and measure the number of flips before the system settles on a stable state. (c-d) Ensemble averaged transient  $\langle \tau \rangle$ , where  $\tau$  is the number of cyclic drive cycles after which the system reaches a periodic orbit (Supplemental Material).

self-loops.

*Strict ensembles.*— We now present ensembles of asymmetric interactions which are not governed by a decreasing pseudo energy yet strictly prohibit self-loops. First, if all interactions are positive ( $c_{ij} \geq 0$ ), avalanches exhibit monotonic evolution of the magnetization  $m := \Sigma s_i$ , thus prohibiting self-loops (Appendix B). If all interactions are negative, and either  $c_{ik} = -d_k$  (constant-columns) or  $c_{ki} = -d_k$  (constant-rows), where  $d_k \geq 0$ , self-loops are also prohibited. In the former case, the interactions prohibit scrambling [12], which in turn prohibits self-loops (Appendix C); in the latter case, the interactions only allow avalanches of length two, too short to form a self-loop (Appendix D and Supplemental Material).

The strictly self-loop-free ensembles allow us to study the statistics of unprecedentedly large systems of interacting hysterons, including the distributions of avalanche sizes  $A$ , transient times  $\tau$ , and multiperiodicities  $T$  of orbits under cyclic drive (Fig. 4; see Supplemental Material). We find that these depend on the ensemble, e.g., avalanches and transients are shorter in the constant-columns ensemble than in the symmetric ensemble, and their dependence on  $NJ_0$  is qualitatively different. These differences underscore the need to define ensembles based on the properties of the underlying physical system.

*Discussion.*— Self-loops are forbidden in dissipative systems and an important feature of active systems [42, 47]. As the parameter regions where self-loops oc-

cur form a vast cloud of complex polytopes, it is unlikely that simple, precise expressions can be found to distinguish regions with and without self-loops. We introduce lenient and strict ensembles, and note that the reciprocal, WA, and strictly positive or constant-columns interactions can be realized experimentally [5, 12, 26, 28], but not the constant-rows ensemble (Supplemental Material). More generally, we propose exploring explicit mappings from physical models to hysteron models, because ensembles derived from well-behaved models, like overdamped bistable springs, are guaranteed to be self-loop free [7, 12, 26, 48].

Second, the statistics of, e.g., avalanches and self-loops, drastically depends on the dynamical rule, which also arises from the underlying physics. In particular, when race conditions are not allowed [12, 21, 31], constant-columns interactions restrict the avalanche size  $A \leq 2$ , whereas flipping the most (or least) unstable elements leads to much larger  $A$  (Fig. 4-a); moreover, flipping all unstable elements leads to a dominance of  $L = 2$  self-loops for symmetric, constant-columns and constant-rows interactions (see Supplemental Material). Hence, physical mappings are a compelling subject for further investigation.

We conclude this paper by proposing three additional directions for future research. First, we suggest that self-loops and multiperiodic responses under cyclic driving [5] have links that can be revealed using the recently introduced concept of the transition scaffold [31]. For example, an orbit of period  $T = 3$  can be constructed based on an appropriate self-loop (Fig. S9c-right). Second, noting that 2D networks of bistable springs can be mapped to strongly asymmetric hysterons models without self-loops, we encourage studying the conditions for weak and strong asymmetry [26]. Finally, our goal to prevent self-loops is mirrored in recent works that aim to understand non-reciprocal phase transitions, and we suggest investigating other interaction ensembles (like WA, constant-columns, or otherwise derived from an underlying model) in this context [41, 42, 47].

## Acknowledgments

PB and MvH acknowledge funding from European Research Council Grant ERC-101019474. We thank Dor Shohat, Yoav Lahini, Corentin Coulais and Menachem Stern for useful discussions.

## Appendix A: Systematic convergence for symmetric couplings.

In this section, we focus on symmetric couplings and demonstrate that correctly initiated avalanches are systematically finite and terminate on a stable state. Moreover, for the sake of simplicity, we focus on the case of spins, i.e. the spans  $\sigma_i$  of the elements are all zero. Thus,  $h_i^+ = h_i^- = h_i^c$ .



Let us consider an initial state  $S^0$ , and a value of the drive  $U$  such that element  $p$  is unstable. The instability condition yields:

- $H > h_p^c - \sum_{j \neq p} s_j^0 c_{pj}$ , if  $s_p^0 = -1$ .
- $H < h_p^c - \sum_{j \neq p} s_j^0 c_{pj}$ , if  $s_p^0 = 1$ .

Therefore, element  $p$  is unstable in state  $S^0$  when:

$$s_p^0 \left( H - h_p^c + \sum_{j \neq p} s_j^0 c_{pj} \right) < 0. \quad (\text{A1})$$

Let us now introduce the function  $V$ , mapping with the total energy of a Sherrington-Kirkpatrick model with

random fields:

$$\begin{aligned} V(\mathbf{s}) &= - \sum_i \left[ s_i (H - h_i^c) + \frac{1}{2} \sum_{j \neq i} s_i s_j c_{ij} \right], \\ &= - \sum_i s_i \left[ H - h_i^c + \frac{1}{2} \sum_{j \neq i} s_j c_{ij} \right], \end{aligned} \quad (\text{A2})$$

where the first (resp. second) term on the r.h.s. of Eq. (A2) can be seen as a field (resp. interaction) term. We want to compute  $\Delta V = V(S^1) - V(S^0)$ , where  $S^1$  is the state of the system after the snap of element  $p$ , i.e.  $s_{i \neq p}^1 = s_{i \neq p}^0$ , and  $s_p^1 = -s_p^0$ . Let us compute  $V(S^1)$ :

$$\begin{aligned} V(S^1) &= - \sum_i s_i^1 (H - h_i^c) - \frac{1}{2} \sum_i \sum_{i \neq j} s_i^1 s_j^1 c_{ij}, \\ &= - \sum_i s_i^0 (H - h_i^c) - \frac{1}{2} \sum_i \sum_{i \neq j} s_i^0 s_j^0 c_{ij} + 2s_p^0 (H - h_p^c) + s_p^0 \sum_{j \neq p} s_j^0 (c_{jp} + c_{pj}). \end{aligned} \quad (\text{A3})$$

Thus

$$\Delta V = 2s_p^0 \left[ (H - h_p^c) + \frac{1}{2} \sum_{j \neq p} s_j^0 (c_{jp} + c_{pj}) \right]. \quad (\text{A4})$$

Finally, invoking symmetric interactions, i.e.  $c_{jp} = c_{pj}$ , we find:

$$\Delta V = 2s_p^0 \left[ (H - h_p^c) + \sum_{j \neq p} s_j^0 c_{pj} \right]. \quad (\text{A5})$$

Inserting the instability condition for hysteron  $p$  yields  $\Delta V < 0$ . Therefore, the function  $V$  is monotonically decreasing for each single snap corresponding to an unstable element. Given the function  $V$  is bounded from below, the system cannot be trapped in a self-loop and must always converge toward a stable state. Note the importance of the factor 1/2 in Eq. (A2) in order to obtain the final result. The demonstration can be extended to finite span hysterons with little effort, which is confirmed by measuring the evolution of  $V$  as given by Eq. (2) in numerical simulations.

### Appendix B: Systematic convergence for purely ferromagnetic couplings.

In this section, we show that for purely ferromagnetic couplings, i.e.  $c_{ij} > 0$ , the system cannot get trapped into a self-loop.

Remember that self-loops corresponds to cyclic

avalanches: the system must come back to a previously visited unstable state. We have seen above that for purely antiferromagnetic couplings, avalanches must be composed of alternating up and down (elementary) transitions [21, 49]. Conversely, for purely ferromagnetic couplings, avalanches are composed of (elementary) transitions which all go in the same direction, i.e. the magnetization evolves monotonically during avalanches. Therefore, when a transition is initiated starting from a stable state, the magnetization cannot revisit its value at a previously visited state, preventing the system to get trapped into a self-loop. Remarkably, the same reasoning applies to show that self-loops are forbidden for purely ferromagnetic interactions when race conditions are resolved by snapping all unstable hysterons simultaneously (Supplemental Material).

### Appendix C: Systematic convergence for constant-columns couplings.

In this section, we elaborate on the reason why constant-columns couplings ( $c_{ik} = -d_k$ ,  $d_k \geq 0$ ) lead to self-loop-free models.

First, remember that for purely antiferromagnetic couplings, avalanches (including self-loops) must be composed of alternating up/down transitions. For all  $L \geq 6$ , there exists at least one self-loop involving only alternating up/down transitions (see Fig. S9-c, right, and Supplemental Material). All these self-loops are in principle allowed in the presence of purely antiferromagnetic interactions. Importantly, however, all such self-loops violate loop-RPM, which requires scrambling: the ordering of

the switching fields must be state-dependent. It was recently shown that the structure of the interaction matrix of constant-columns couplings prevents any scrambling from happening [12], i.e. the ordering of the switching field is the same for all states. This is the reason why self-loops of any size are forbidden for constant-columns couplings.

#### Appendix D: Systematic convergence for constant-rows couplings.

In this section, we show that for constant-rows couplings ( $c_{ki} = -d_k$ ,  $d_k \geq 0$ ), avalanches systematically stop on a stable state after one or two snaps.

Let us consider a stable state  $S^0$  at the edge of instability, i.e. there is a marginally stable element, denoted  $p$ , such that  $H = H_p^+(S^0)$  if  $s_p^0 = -1$  (resp.  $H = H_p^-(S^0)$  if  $s_p^0 = +1$ ), and all the other elements are stable. We denote the distances to the instability of the different elements  $\Delta H_i(S^0)$ , where  $\Delta H_p(S^0) = 0$ , and  $\Delta H_{i \neq p}(S^0) > 0$ . At this point, any infinitesimal increase (or decrease, depending on  $s_p^0$ ) of  $H$  destabilizes element  $p$ , which snaps from  $s_p^0$  to  $-s_p^0$ , leading to state  $S^1$ . The distances to instability in this state write  $\Delta H_{i \neq p}(S^1) = \Delta H_i(S^0) + 2s_i^0 s_p^0 d_i$ , and  $\Delta H_p(S^1) = \sigma_p > 0$ . Therefore, in general, many elements are unstable in state  $S^1$ , especially those with large  $d_i$ , and opposite initial signs. Remarkably, avalanches must be composed of alternating up and down (elementary) transitions when the interactions are purely antiferromagnetic [21, 49], which is the case of constant-rows couplings. Let us analyze separately the

cases of different numbers of unstable elements in state  $S^1$ :

- If no element are unstable,  $S^1$  is stable, and the avalanche is a trivial Preisach-like transition of size 1.
- If a single element is unstable, say hysteron  $q \neq p$ ,  $S^1$  is unstable and element  $q$  snaps, leading to state  $S^2$ . Importantly, element  $q$  has a different value in state  $S^0$  than element  $p$ , i.e.  $s_q^0 = -s_p^0$  [21, 49]. In the new state, the distances to instability of all the other elements then write  $\Delta H_{i \neq p,q}(S^2) = \Delta H_i(S^0) + 2s_i^0 s_p^0 d_i + 2s_i^0 s_q^0 d_i = \Delta H_i(S^0) > 0$ , thus they are all stable, with the same distances to instability as in state  $S^0$ . The distance to instability of element  $p$  writes  $\Delta H_p(S^2) = \Delta H_p(S^1) + 2s_p^1 s_q^1 d_p > \Delta H_p(S^1) > 0$ , and the distance to instability of element  $q$  writes  $\Delta H_q(S^2) = -\Delta H_q(S^1) + \sigma_q > 0$ . Thus all elements are stable in state  $S^2$  and the avalanche must stop.
- If multiple elements are unstable, we denote  $q \neq p$  the index of the most unstable one, and apply the same reasoning as above. Crucially, the same reasoning applies for the other race condition rules where elements flip one by one (Supplemental Material).

Altogether, avalanches must stop after a maximum of two snaps, preventing the system from falling into a self-loop, and guaranteeing to find a stable state for all values of  $H$ .

- 
- [1] F. Preisach, *Zeitschrift für physik* **94**, 277 (1935).
- [2] N. C. Keim, J. D. Paulsen, Z. Zeravcic, S. Sastry, and S. R. Nagel, *Reviews of Modern Physics* **91**, 035002 (2019).
- [3] J. D. Paulsen and N. C. Keim, *Proceedings of the Royal Society A* **475**, 20180874 (2019).
- [4] C. W. Lindeman and S. R. Nagel, *Science Advances* **7**, eabg7133 (2021).
- [5] N. C. Keim and J. D. Paulsen, *Science Advances* **7**, eabg7685 (2021).
- [6] T. Jules, A. Reid, K. E. Daniels, M. Mungan, and F. Lechenault, *Physical Review Research* **4**, 013128 (2022).
- [7] D. Shohat, D. Hexner, and Y. Lahini, *Proceedings of the National Academy of Sciences* **119**, e2200028119 (2022).
- [8] N. C. Keim and D. Medina, *Science Advances* **8**, eabo1614 (2022).
- [9] J. D. Paulsen and N. C. Keim, *arXiv preprint arXiv:2405.08158* (2024).
- [10] H. Bense and M. van Hecke, *Proceedings of the National Academy of Sciences* **118**, e2111436118 (2021).
- [11] L. J. Kwakernaak and M. van Hecke, *Physical Review Letters* **130**, 268204 (2023).
- [12] J. Liu, M. Teunisse, G. Korovin, I. R. Vermaire, L. Jin, H. Bense, and M. van Hecke, *Proceedings of the National Academy of Sciences* **121**, e2308414121 (2024).
- [13] D. Melancon, A. E. Forte, L. M. Kamp, B. Gorissen, and K. Bertoldi, *Advanced Functional Materials* **32**, 2201891 (2022).
- [14] A. Meeussen and M. van Hecke, *Nature* **621**, 516 (2023).
- [15] M. Brandenbourger, C. Scheibner, J. Veenstra, V. Vitelli, and C. Coulais, *arXiv preprint arXiv:2108.08837* (2021).
- [16] J. Veenstra, O. Gamayun, X. Guo, A. Sarvi, C. V. Meinersen, and C. Coulais, *Nature* **627**, 528 (2024).
- [17] L. M. Kamp, M. Zanaty, A. Zareei, B. Gorissen, R. J. Wood, and K. Bertoldi, *arXiv preprint arXiv:2409.03737* (2024).
- [18] M. Mungan, S. Sastry, K. Dahmen, and I. Regev, *Physical review letters* **123**, 178002 (2019).
- [19] M. Mungan and M. M. Terzi, in *Annales Henri Poincaré*, Vol. 20 (Springer, 2019) pp. 2819–2872.
- [20] M. M. Terzi and M. Mungan, *Physical Review E* **102**, 012122 (2020).
- [21] M. van Hecke, *Physical Review E* **104**, 054608 (2021).
- [22] G. Puglisi and L. Truskinovsky, *Journal of the Mechanics and Physics of Solids* **48**, 1 (2000).
- [23] A. Nicolas, E. E. Ferrero, K. Martens, and J.-L. Barrat, *Reviews of Modern Physics* **90**, 045006 (2018).
- [24] D. Kumar, S. Patinet, C. E. Maloney, I. Regev, D. Vandembroucq, and M. Mungan, *The Journal of Chemical*

- Physics **157** (2022).
- [25] D. Kumar, M. Mungan, S. Patinet, and D. Vandembroucq, arXiv preprint arXiv:2409.07621 (2024).
  - [26] D. Shohat and M. van Hecke, arXiv preprint arXiv:2409.07804 (2024).
  - [27] J. Ding and M. van Hecke, The Journal of Chemical Physics **156** (2022).
  - [28] J. D. Paulsen, arXiv preprint arXiv:2409.07726 (2024).
  - [29] N. C. Keim, J. Hass, B. Kroger, and D. Wieker, Physical Review Research **2**, 012004 (2020).
  - [30] C. W. Lindeman, T. R. Jalowiec, and N. C. Keim, arXiv preprint arXiv:2306.07177 (2023).
  - [31] M. H. Teunisse and M. van Hecke, arXiv preprint arXiv:2404.11344 (2024).
  - [32] H. Gutfreund, J. Reger, and A. Young, Journal of Physics A: Mathematical and General **21**, 2775 (1988).
  - [33] K. Nutzel and U. Krey, Journal of Physics A: Mathematical and General **26**, L591 (1993).
  - [34] H. Eissfeller and M. Opper, Physical Review E **50**, 709 (1994).
  - [35] S. Hwang, V. Folli, E. Lanza, G. Parisi, G. Ruocco, and F. Zamponi, Journal of Statistical Mechanics: Theory and Experiment **2019**, 053402 (2019).
  - [36] C. Coulais, D. Sounas, and A. Alu, Nature **542**, 461 (2017).
  - [37] S. Kirkpatrick and D. Sherrington, Physical Review B **17**, 4384 (1978).
  - [38] J. J. Hopfield, Proceedings of the national academy of sciences **79**, 2554 (1982).
  - [39] A. Crisanti and H. Sompolinsky, Physical Review A **36**, 4922 (1987).
  - [40] D. Panchenko, *The sherrington-kirkpatrick model* (Springer Science & Business Media, 2013).
  - [41] M. Fruchart, R. Hanai, P. B. Littlewood, and V. Vitelli, Nature **592**, 363 (2021).
  - [42] G. G. Lorenzana, A. Altieri, G. Biroli, M. Fruchart, and V. Vitelli, arXiv preprint arXiv:2408.17360 (2024).
  - [43] G. Parisi, Fractals **11**, 161 (2003).
  - [44] M. B. Jesi, *Spin Glasses: Criticality and Energy Landscapes* (Springer, 2016).
  - [45] D. E. Knuth, in *The art of computer programming: fundamental algorithms* (1975) pp. 634–634.
  - [46] M. Deza and R. Shklyar, arXiv preprint arXiv:1003.4391 (2010).
  - [47] Y. Avni, M. Fruchart, D. Martin, D. Seara, and V. Vitelli, arXiv preprint arXiv:2409.07481 (2024).
  - [48] D. Shohat, Y. Friedman, and Y. Lahini, Nature Physics **19**, 1890 (2023).
  - [49] J. P. Sethna, K. Dahmen, S. Kartha, J. A. Krumhansl, B. W. Roberts, and J. D. Shore, Physical Review Letters **70**, 3347 (1993).

# Supplemental Material: Proliferation and prevention of self-loops in ensembles of interacting binary elements

Paul Baconnier<sup>1</sup>, Margot H. Teunisse<sup>1,2</sup> and Martin van Hecke<sup>1,2</sup>

<sup>1</sup>*AMOLF, 1098 XG Amsterdam, The Netherlands.*

<sup>2</sup>*Huygens-Kamerlingh Onnes Laboratory, Leiden University, 2300 RA Leiden, The Netherlands.*

In the main manuscript, we investigate the root causes and statistics of self-loops in ensembles of interacting binary elements, and we find several strict ensembles that are completely free of self-loops.

In this document, we first elaborate on the conditions under which a self-loop emerges in the transition-graph shown in Fig. 1 of the main text. In Secs. 2 and 3, we show the probability of race conditions and the probability that a given state has a finite stability range as a function of coupling strength, for randomly-coupled spins and hysterons. In Secs. 4 and 5, we provide numerical evidence that the same problems of overwhelming self-loops holds if one considers spins instead of hysterons, and for ensembles of hysterons with equal spans. In Sec. 6, we further analyze the relationship between gaps and self-loops. In Sec. 7, we provide numerical evidence that self-loops also overwhelm the response of large systems in the case of weakly asymmetric interactions. In Sec. 8, we derive the conditions to prevent  $L = 4$  self-loops for  $N = 2$  spins and  $N = 2$  hysterons with equal spans, and sample  $L = 4$  self-loops for large  $N$ . In Sec. 9, we provide physical illustrations for the different classes of well-behaved models. In Sec. 10, we analyze the role of the different race conditions rules in the different families of models. In Sec. 11, we give details on the algorithm to generate all possible self-loops, and illustrate the different possible self-loop structures for different sizes  $L$ . Finally, in Sec. 12, we illustrate a few numerical simulations of large systems of well-behaved models.

## 1: Conditions for a self-loop of size 4 in the general model

In this section, we elaborate on the conditions under which a self-loop emerges in the graph represented in Fig. 1 of the main text.

The first condition is that there exists a range of  $H$  inside which all the states  $S^0$ ,  $S^1$ ,  $S^2$  and  $S^3$  are unstable. This situation is realized when  $H$  is larger than the two up switching fields  $H^+(S^0)$  and  $H^+(S^1)$ , and smaller than the two down switching fields  $H^-(S^2)$  and  $H^-(S^3)$ , so that a self-loop can emerge only when both  $H^+(S^0)$  and  $H^+(S^1)$  are smaller than  $H^-(S^2)$  and  $H^-(S^3)$ .

The actual question one should ask is: starting from a stable state and driving the system up to instability, what are the conditions under which the transition triggers a self-loop? In this case, we evaluate the possibility for a self-loop for  $H$  immediately above(/below) the up(/down) switching field of a given state. For each of the four possible starting states, we can write down the inequalities needed so that the loop shown on Fig. 1 of the main text is realized:

- **State  $S^0$ :** this state becomes unstable as soon as  $H > H^+(S^0)$ , and a self-loop emerges at instability only when:

$$\begin{aligned} H^+(S^1) &< H^+(S^0), \\ H^-(S^2) &> H^+(S^0), \\ H^-(S^3) &> H^+(S^0), \end{aligned} \tag{S1}$$

where each relationship enforces that a given state of the loop is unstable. The conditions under which the transition triggers a self-loop write:  $H^+(S^1) < H^+(S^0) < H^-(S^2), H^-(S^3)$ . This is the relationship provided in the caption of Fig. 1 of the main text.

- **State  $S^1$ :** this state becomes unstable as soon as  $H > H^+(S^1)$ , and a self-loop emerges at instability only when:

$$\begin{aligned} H^+(S^0) &< H^+(S^1), \\ H^-(S^2) &> H^+(S^1), \\ H^-(S^3) &> H^+(S^1). \end{aligned} \tag{S2}$$

The conditions under which the transition triggers a self-loop write:  $H^+(S^0) < H^+(S^1) < H^-(S^2), H^-(S^3)$ .



- **State  $S^2$** : this state becomes unstable as soon as  $H < H^-(S^2)$ , and a self-loop emerges at instability only when:

$$\begin{aligned} H^-(S^3) &> H^-(S^2), \\ H^+(S^0) &< H^-(S^2), \\ H^+(S^1) &< H^-(S^2). \end{aligned} \tag{S3}$$

The conditions under which the transition triggers a self-loop write:  $H^+(S^0), H^+(S^1) < H^-(S^2) < H^-(S^3)$ .

- **State  $S^3$** : this state becomes unstable as soon as  $H < H^-(S^3)$ , and a self-loop emerges at instability only when:

$$\begin{aligned} H^-(S^2) &> H^-(S^3), \\ H^+(S^0) &< H^-(S^3), \\ H^+(S^1) &< H^-(S^3). \end{aligned} \tag{S4}$$

The conditions under which the transition triggers a self-loop write:  $H^+(S^0), H^+(S^1) < H^-(S^3) < H^-(S^2)$ .

As one can be seen from the conditions above, self-loops arise under different conditions depending on the starting state.

## 2: Race conditions

In this section, we measure the probability of race conditions for collections of spins ( $\sigma_i = 0$ ), hysterons ( $\sigma_i$  flatly sampled from  $[0, 0.5]$ ), and hysterons with equal spans ( $\sigma_i = 0.5$ ).

When a state  $S^0$  becomes unstable and one of the hysterons flips to produce state  $S^1$ , the number of unstable hysterons in  $S^1$  can be either zero ( $S^1$  is stable), one, or more than one. If more than one hysteron is unstable, this causes a race condition, which requires to define a dynamical rule specifying which unstable element flips first.

We calculate the race-condition probability  $P_{RC}$  – the probability of more than one hysteron being unstable in state  $S^1$  – by selecting a state  $S^0$  that is stable at  $H = 0$ , increasing  $H$  past  $H^+(S^0)$ , and investigating the number of unstable hysterons of  $S^1$  at  $H = H^+(S^0)$ . We find that  $P_{RC}$  increases as  $(NJ_0)^2$  for  $NJ_0 \ll 1$ , and saturates at a significant value that increases towards 1 for large  $N$  for  $NJ_0 \gg 1$  (Figs. S1). We find only minor differences between spins, hysterons, and hysterons with equal spans, though the data suggest that race conditions are more likely for spins.

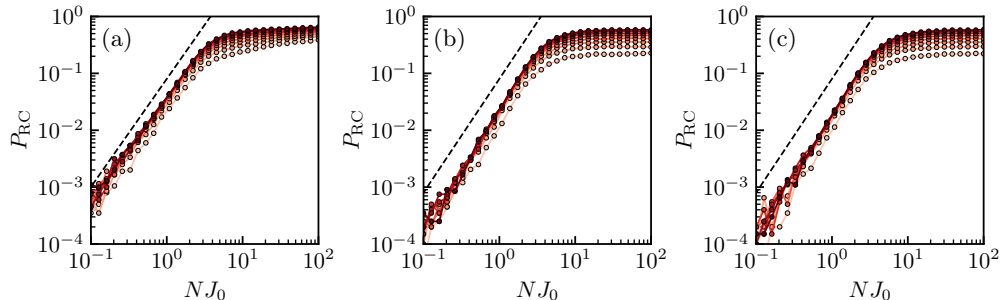


FIG. S1: **Statistics of race conditions for randomly-coupled two-states elements.** Probability  $P_{RC}$  of race conditions (ensemble of  $2 \times 10^4$  transitions  $S^0 \rightarrow S^1$ ), for an initial state  $S^0$  stable at  $H = 0$ ; the black dashed line represents the slope 2. Markers are color coded from light to dark red as  $N$  increases, with  $N \in [2, 3, 4, 5, 6, 7, 8, 9, 10]$ . (a) Spins ( $\sigma_i = 0$ ). (b) Hysterons ( $\sigma_i$  flatly sampled from  $[0, 0.5]$ ). (c) Hysterons with equal spans ( $\sigma_i = 0.5$ ).

## 3: Number of stable states

In this section, we measure the probability that a given state has a finite stability range for collections of spins ( $\sigma_i = 0$ ), hysterons ( $\sigma_i$  flatly sampled from  $[0, 0.5]$ ), and hysterons with equal spans ( $\sigma_i = 0.5$ ).

Independently of the microscopic hysteresis and coupling strength, the probability  $P_s$  that a random state  $S$  among the  $2^N$  possible states is stable for some value of the driving  $H$ , i.e.  $H^+(S) > H^-(S)$ , asymptotes to 0 for large

$N$ . Indeed, for spins, it is easy to show that there always exists only  $N + 1$  potentially stable states, so that  $P_s = P_{\text{spins}} = (N + 1)/2^N$  (Fig. S2-a).

For hysterons and hysterons with equal spans, we find that  $P_s$  asymptotes toward  $P_{\text{spins}}$  in the large coupling limit, i.e.  $NJ_0 \gg 1$  (Figs. S2-b and c). However, in the small coupling limit,  $P_s$  is larger than  $P_{\text{spins}}$ . In this case,  $P_s$  is dictated by the statistics of the Preisach graphs that are sampled, which is itself dictated by the statistics of the different orderings of the switching fields  $h_i^\pm$ . Interestingly, in the case of hysterons with equal spans, the Preisach graphs which are sampled generally contain more stable states. Note that in all case,  $P_s$  still asymptotes to 0 even in the small coupling limit, but slower than in the case of spins.

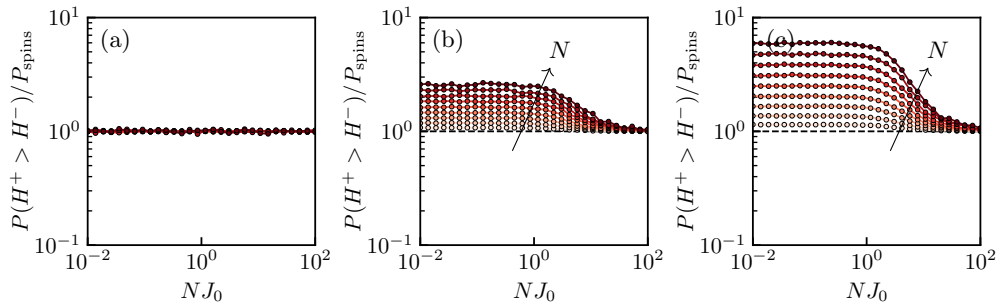


FIG. S2: **Fraction of potentially stable states.** Probability that a randomly chosen state  $S$  has a finite stability range; scaled by  $P_{\text{spins}} = (N + 1)/2^N$ . Markers are color coded from light to dark red as  $N$  increases, with  $N \in [2, 3, 4, 5, 6, 7, 8, 9, 10]$ . (a) Spins ( $\sigma_i = 0$ ). (b) Hysterons ( $\sigma_i$  flatly sampled from  $[0, 0.5]$ ). (c) Hysterons with equal spans ( $\sigma_i = 0.5$ ).

#### 4: Case of binary spins

In this section, we reproduce the simulations of Fig. 2 of the main text, focusing on the case of randomly-coupled spins, i.e.  $\sigma_i = 0$  for all the elements (Figs. S3).

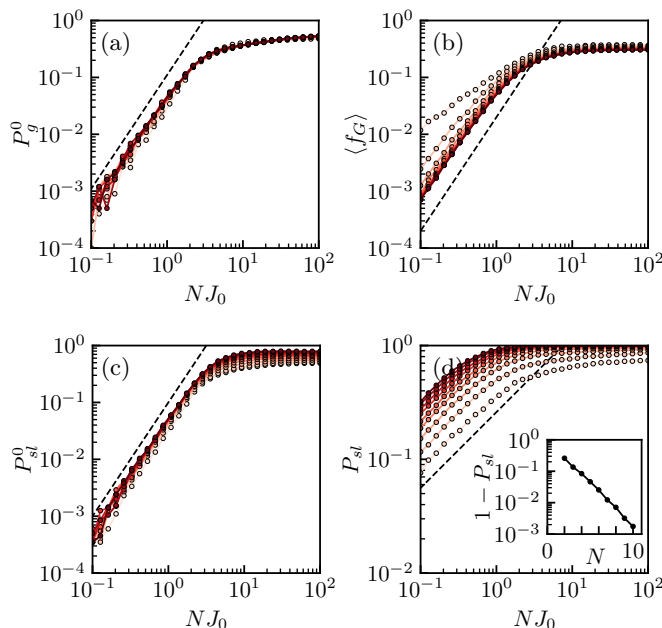


FIG. S3: **Overwhelming self-loops for randomly-coupled spins.** Statistical measures for gaps and self loops scale when plotted as function of  $NJ_0$  and dominate for  $NJ_0 \gg 1$  ( $10^5$  samples; color from light to dark as  $N$  increases from 2 to 10). (a) Probability  $P_g^0$  of finding a gap at  $H = 0$  (dashed line indicates slope 2). (b) Fraction of gaps  $f_g$ , defined as the mean of the ratio of the size of intervals where no stable states exist divided by  $[H^+(-\dots-), H^- (+\dots+)]$  (dashed line indicates slope 2). (c) Probability  $P_{sl}^0$  of self-loops at  $H = 0$  (dashed line indicates slope 2). (d) Probability  $P_{sl}$  of finding at least one self-loop for any value of  $H$  (dashed line indicates slope  $2/3$ ). Inset: The probability to be self-loop free,  $1 - P_{sl}$ , decays to zero exponentially with  $N$  for large couplings ( $NJ_0 = 10^2$ ).

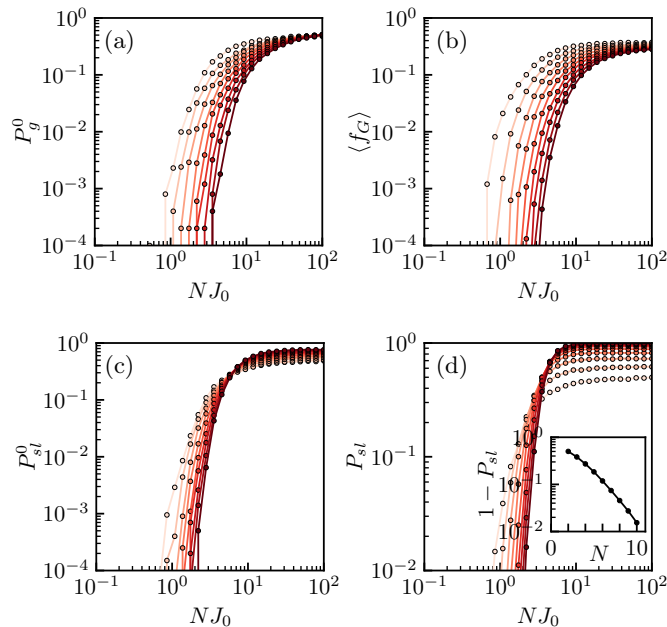


FIG. S4: **Overwhelming self-loops for randomly-coupled hysterons with equal spans.** Statistical measures for gaps and self loops scale when plotted as function of  $NJ_0$  and dominate for  $NJ_0 \gg 1$  ( $10^5$  samples; color from light to dark as  $N$  increases from 2 to 10). (a) Probability  $P_g^0$  of finding a gap at  $H = 0$ . (b) Fraction of gaps  $f_g$ , defined as the mean of the ratio of the size of intervals where no stable states exist divided by  $[H^+(-\dots-), H^-(+\dots+)]$ . (c) Probability  $P_{sl}^0$  of self-loops at  $H = 0$ . (d) Probability  $P_{sl}$  of finding at least one self-loop for any value of  $H$ . Inset: The probability to be self-loop free,  $1 - P_{sl}$ , decays to zero exponentially with  $N$  for large couplings ( $NJ_0 = 10^2$ ).

Let us focus on the similarities with the case of hysterons with distributed spans. As for hysterons, the statistical weight of gaps increases as a power law for  $NJ_0 \ll 1$ , and saturates toward a significant value for  $NJ_0 \gg 1$  (Figs. S3-a and b). Moreover, the probability of finding at least one self-loop for any  $H$  increases as a power law for  $NJ_0 \ll 1$ , and saturates toward a constant value for  $NJ_0 \gg 1$  (Fig. S3-d), which asymptotes to 1 as  $N$  increases (Fig. S3-d, inset). Therefore, the same way as for hysterons, the response of large, strongly coupled systems of spins is dominated by self-loops.

There are however differences with the case of hysterons. In particular, all observables grow slower with  $NJ_0$  than for hysterons for  $NJ_0 \ll 1$  (there are more gaps and self-loops for spins than for hysterons for a given  $NJ_0 \ll 1$ ). Also, for  $NJ_0 \gg 1$ , self-loops are more likely with spins than with hysterons: for  $N = 10$  and in the large coupling limit ( $NJ_0 = 10^2$ ), 99.8% of instances exhibit at least one self-loop for spins, while the probability is 98.5% for hysterons. This is expected given the microscopic hysteresis contributes to prevent loops that would be possible otherwise.

### 5: Case of hysterons with equal spans

In this section, we reproduce the simulations of Fig. 2 of the main text, focusing on the case of randomly-coupled hysterons with equal spans, i.e.  $\sigma_i = 0.5$  for all the elements (Figs. S4).

We again start by discussing similarities with the case of hysterons with distributed spans. Most importantly, we find that the probability of finding at least one self-loops for any  $H$  saturates toward a constant value for  $NJ_0 \gg 1$  (Fig. S4-d), which asymptotes to 1 as  $N$  increases (Fig. S4-d, inset)

However, in the case of hysterons with equal spans, we find that all observables seem to have a lower cutoff in  $NJ_0$  below which no gaps or self-loops exist. This is expected given the physics of self-loops for  $N = 2$  hysterons (see Fig. 3-d of the main text and next section). Moreover, also as expected, we find an even lower probability of 98.3% of finding at least one self-loop for any  $H$  for  $N = 10$  and  $NJ_0 = 10^2$  (Fig. S4-d).

### 6: Relationship between gap and self-loops

In this section, we provide further evidence that inside a gap all initial conditions get trapped into self-loops, and that self-loops can occur outside of gaps. We restrict to  $H = 0$ , and we measure the probability of finding a gap  $P_g^0$ , and of the emergence of at least one self-loop starting from any of the  $2^N$  states  $P_{sl}^0$ , from zero to large  $J_0$ .

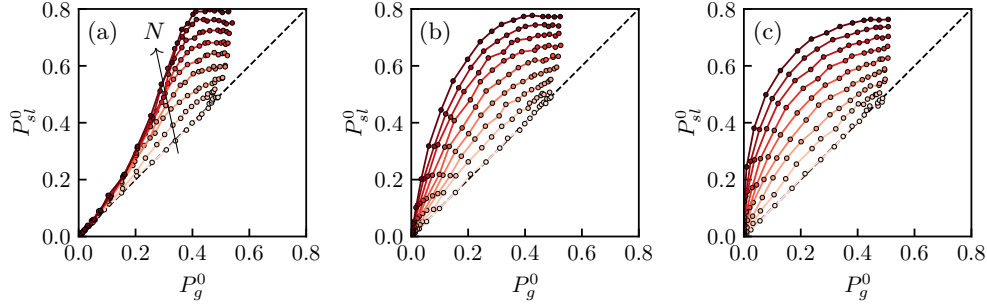


FIG. S5: **Probability of self-loops as a function of the probability of gaps** at  $H = 0$ , for  $NJ_0 \in [10^{-1}, 10^2]$ . (a) Spins ( $\sigma_i = 0$ ). (b) Hysterons with distributed spans ( $\sigma_i$  flatly sampled from  $[0, 0.5]$ ). (c) Hysterons with equal spans ( $\sigma_i = 0.5$ ). The black dashed lines represent  $y = x$ ; markers are color coded from light to dark red as  $N$  increases, with  $N \in [2, 3, 4, 5, 6, 7, 8, 9, 10]$ .

For  $N = 2$  spins (Fig. S5-a), hysterons (Fig. S5-b), and hysterons with equal spans (Fig. S5-c), there is a one-to-by correspondence between the probability of gaps  $P_g^0$  and the probability of self-loops  $P_{sl}^0$ : indeed, in this case, all 4 possible states must be unstable to lead to a self-loop. However, for larger  $N$ , we systematically find more self-loops than gaps. The larger  $N$  and the larger the coupling  $J_0$ , the larger the weight of self-loops as compared to gaps. Interestingly, in the limit of small couplings, for spins the data suggest that self-loops and gaps remain equally likely. In contrast, for hysterons, the larger  $N$ , the larger the weight of self-loops.

## 7: Weak asymmetry

In this section, we reproduce the simulations of Fig. 2 of the main text, focusing on the case of hysterons with distributed spans ( $\sigma_i$  flatly sampled from  $[0, 0.5]$ ), and restricted to weakly asymmetric interactions, i.e.  $c_{ij}c_{ji} > 0$  for all pairs  $(i, j)$  (Figs. S6).

There are two main differences with purely random couplings. First, the probability  $P_{sl}^0$  of at least one self-loop occurring at  $H = 0$  saturates toward a constant value for  $NJ_0 \gg 1$  (Fig. S6-a), which decreases with  $N$ . Strikingly, the larger the system, the less likely are self-loops to occur at  $H = 0$ . Moreover, the probability  $P_{sl}$  of finding at least

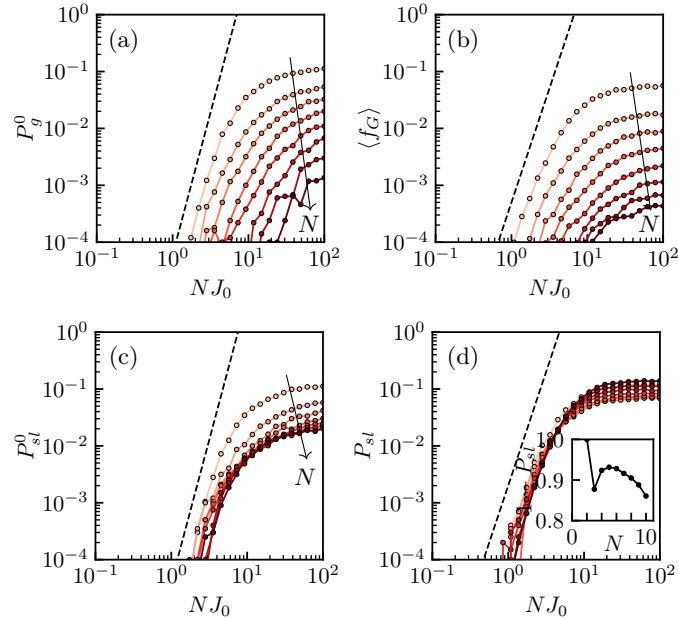


FIG. S6: **Overwhelming self-loops for weak asymmetric couplings between hysterons.** Statistical measures for self loops scale when plotted as function of  $NJ_0$  ( $10^5$  samples; color from light to dark as  $N$  increases from 2 to 10). (a) Probability  $P_g^0$  of finding a gap at  $H = 0$  (dashed line indicates slope 5). (b) Fraction of gaps  $f_G$ , defined as the mean of the ratio of the size of intervals where no stable states exist divided by  $H^+(-\dots-), H^- (+\dots+)$  (dashed line indicates slope 4). (c) Probability  $P_{sl}^0$  of self-loops at  $H = 0$  (dashed line indicates slope 5). (d) Probability  $P_{sl}$  of finding at least one self-loop for any value of  $H$ ; the black dashed line represents the slope 4. Inset: The probability to be self-loop free,  $1 - P_{sl}$ , decays monotonously with  $N$  for large enough  $N$ , and for large couplings ( $NJ_0 = 10^2$ ).

one self-loops for any  $H$  saturates toward a constant value for  $NJ_0 \gg 1$  (Fig. S6-b), which does not asymptote to 1 with  $N$  as fast as for purely random interactions, but which increases monotonically with  $N$  for large enough  $N$ . Therefore, weakly asymmetric interactions lead to fewer self-loops than random couplings, but we still expect that self-loops dominate the response of large, strongly coupled systems.

### 8: Self-loops of size 4

In this section, we focus on the emergence of  $L = 4$  self-loops, from  $N = 2$  to large  $N$ .

#### 8.1. Gap formation mechanism for $N = 2$ coupled spins

We consider two coupled spins indexed 1 and 2, such that  $h_1^+ = h_1^- = h_1^c$  and  $h_2^+ = h_2^- = h_2^c$  (i.e.  $\sigma_1 = \sigma_2 = 0$ ). Importantly, the only possible self-loop have size  $L = 4$ , such that the system visits all four possible states in a cycle, and thus the self-loop must occur within a gap. Moreover, we consider  $h_1^c < h_2^c$  by convention. We can compute the upper and lower switching fields of individual spins for each state:

$$\begin{aligned} H_1^+(-) &= h_1^c + c_{12}, \\ H_2^+(-) &= h_2^c + c_{21}, \end{aligned} \tag{S1}$$

$$\begin{aligned} H_1^-(+) &= h_1^c + c_{12}, \\ H_2^-(+) &= h_2^c - c_{21}, \end{aligned} \tag{S2}$$

$$\begin{aligned} H_1^+(-) &= h_1^c - c_{12}, \\ H_2^+(-) &= h_2^c + c_{21}, \end{aligned} \tag{S3}$$

$$\begin{aligned} H_1^-(+) &= h_1^c - c_{12}, \\ H_2^-(+) &= h_2^c - c_{21}. \end{aligned} \tag{S4}$$

In the limit of small couplings ( $|c_{12}|, |c_{21}| \ll \Delta h^c$ , with  $\Delta h^c = h_2^c - h_1^c > 0$ ), the upper and lower switching fields of each state write:

$$H^+(-) = H_1^+(-) = h_1^c + c_{12}, \tag{S5}$$

$$\begin{aligned} H^- (+) &= H_1^- (+) = h_1^c + c_{12}, \\ H^+ (+) &= H_2^+ (+) = h_2^c - c_{21}, \end{aligned} \tag{S6}$$

$$\begin{aligned} H^- (-) &= H_2^- (-) = h_2^c + c_{21}, \\ H^+ (-) &= H_1^+ (-) = h_1^c - c_{12}, \end{aligned} \tag{S7}$$

$$H^- (+) = H_2^- (+) = h_2^c - c_{21}. \tag{S8}$$

Note that  $H^+(-) = H^- (+)$  and  $H^+ (+) = H^- (-)$ : at the two up/down transitions, the upper switching field of the state below coincides with the lower switching field of the state above (Fig. S7-a). Therefore, in the limit of small couplings, the convention  $h_1^c < h_2^c$  enforces the structure of the Preisach graph represented in Fig. S7-a. Moreover, until the zero-coupling ordering of the states  $(-) \leftrightarrow (+) \leftrightarrow (++)$  is preserved, no gap can open, even with finite interactions.

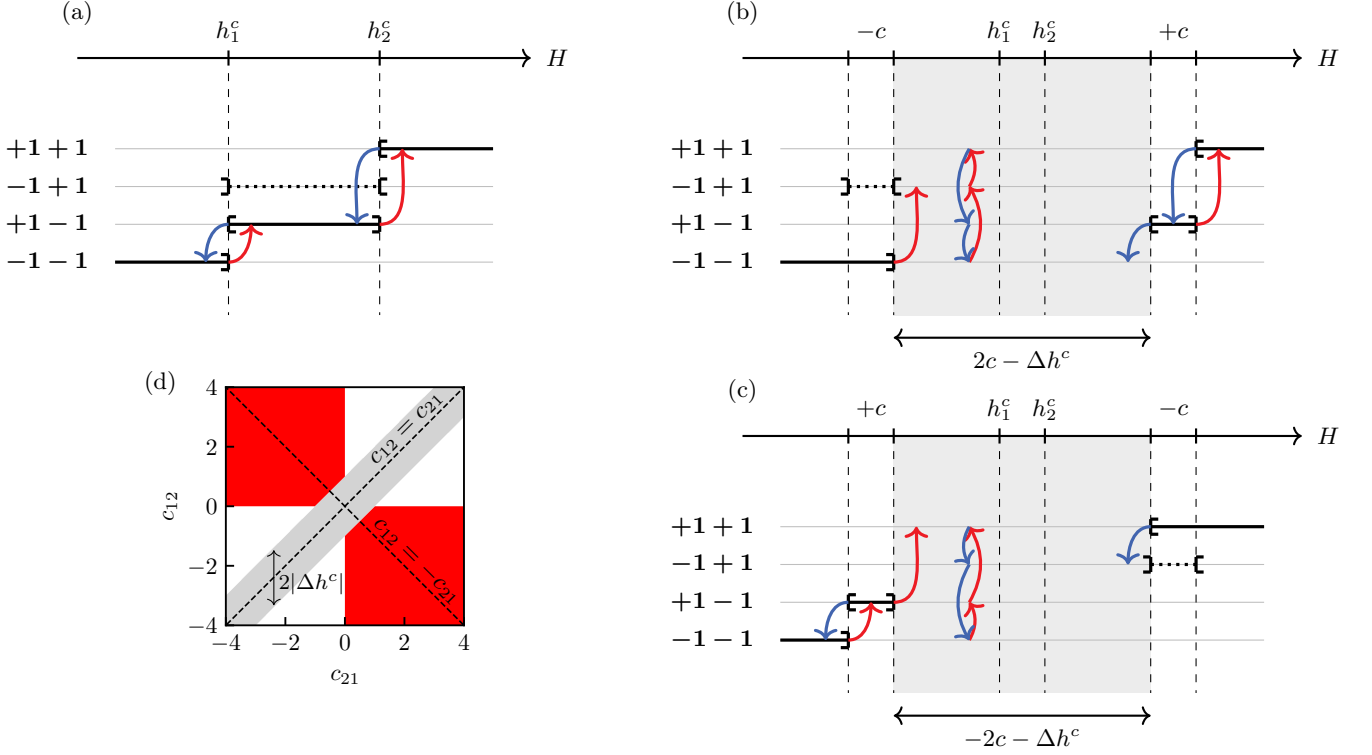


FIG. S7: **Stability ranges for  $N = 2$  binary spins.** (a) No couplings  $c_{12} = c_{21} = 0$ . (b-c) Completely asymmetric couplings  $c_{12} = -c_{21} = c > 0$ , i.e.  $\Delta c > 0$  (b);  $c_{12} = -c_{21} = c < 0$ , i.e.  $\Delta c < 0$  (c). The solid black, dotted black, and solid gray lines represent stable configuration, unstable configuration with 2 unstable spins, and with 1 unstable spin, respectively. Red (resp. blue) arrows represent up (resp. down) transitions. The gray area in (b-c) indicates the range of  $H$  with a gap, and the colored transitions represent the self-loop occurring within this range. (d) Portions of the  $(c_{12}, c_{21})$ -plane leading to  $L = 4$  self-loops (red areas).

One hole may open in two mutually-excluding cases: when the ordering of the switching fields in state  $(--)$  (resp.  $(++)$ ) is reversed. We focus on the first one without loss of generality. The condition  $H_2^+(--) < H_1^+(--)$  translates into:

$$\Delta c > \Delta h^c, \quad (\text{S9})$$

where  $\Delta c = c_{12} - c_{21}$ . Let us assume the condition given by Eq. (S9) is satisfied, and analyze the other states' switching fields. First, the condition to keep the same switching fields ordering in state  $(++)$  can be written as:

$$H_2^-(++) > H_1^-(++) \Leftrightarrow \Delta c > -\Delta h^c, \quad (\text{S10})$$

which is necessarily true when Eq. (S9) is satisfied. Then, the condition to open up a range of  $H$  in between the saturating states' stability ranges writes:

$$H_2^-(++) > H_2^+(--) \Leftrightarrow c_{21} < 0, \quad (\text{S11})$$

imposing the sign of  $c_{21}$ . Finally, we consider the states  $(+-)$  and  $(-+)$ . Let us start with the first one. Given  $H^+(+-) = H^-(++)$ , the opening of a gap inside  $[H^+(--), H^-(++)]$  requires  $H^-(+-) > H^+(--)$ . This condition translates into:

$$H_2^+(--) < H_1^-(+-) \Leftrightarrow \Delta c > \Delta h^c, \quad (\text{S12})$$

which is equivalent to Eq. (S9) characterizing the reversal of the critical hysteron in state  $(--)$ . The last condition to open a gap is that there is a finite range of  $H$  in between  $H^+(+-)$  and  $H^-(+-)$ :



$$H^-(-+) > H^+(-+) \Leftrightarrow c_{12} > 0, \quad (\text{S13})$$

imposing the sign of  $c_{12}$ . Altogether, the necessary and sufficient conditions for the emergence of a self-loop of size  $L = 4$  in a system of  $N = 2$  coupled spins can be written as:

$$\begin{aligned} \Delta c &> \Delta h^c, \\ c_{12}c_{21} &< 0. \end{aligned} \quad (\text{S14})$$

These two conditions lead to the self-loop of size  $L = 4$  represented in Fig. S7-b. The second scenario mentioned above leads to the following conditions:

$$\begin{aligned} \Delta c &< -\Delta h^c, \\ c_{12}c_{21} &< 0, \end{aligned} \quad (\text{S15})$$

which lead to the self-loop of size  $L = 4$  with the opposite chirality, as shown in Fig. S7-c. In conclusion, couplings of opposite signs (strong asymmetry) and large enough asymmetry  $|\Delta c| = |c_{12} - c_{21}|$  lead to a gap in between the saturating states (Fig. S7-d). Inside this gap, no stable state exists, which guarantees the existence of a self-loop of size  $L = 4$ . This is best illustrated by representing the states' stability ranges in the case of completely asymmetric couplings, i.e.  $c_{12} = -c_{21} = c$ , where  $\Delta c = 2c$  (Figs. S7-b and c). We find that a hole of size  $|\Delta c| - |\Delta h^c|$  opens in between the saturating states as soon as  $|\Delta c| > |\Delta h^c|$ .

## 8.2. $N = 2$ coupled hysterons

The conditions above can be extended to the case of hysterons with finite microscopic hysteresis:

$$\begin{aligned} |\Delta c| &> |\Delta h^c + \sigma|, \\ c_{12}c_{21} &< 0, \\ |c_{12}| &> \sigma/2, \\ |c_{21}| &> \sigma/2, \end{aligned} \quad (\text{S16})$$

where we have considered that the two hysterons have the same microscopic hysteresis, i.e.  $\sigma_1 = \sigma_2 = \sigma$ . Expectedly, for larger microscopic dissipation  $\sigma > 0$ , a portion of self-loops that would have been possible for binary spins are forbidden. More precisely, self-loops emerge for larger asymmetry, i.e.  $|\Delta c| > |\Delta h^c + \sigma|$ , and large enough couplings, i.e.  $|c_{12}| > \sigma/2$  and  $|c_{21}| > \sigma/2$ . Note that, the same way as for spins, self-loops emerge only when the coupling coefficients have opposite signs, i.e.  $c_{12}c_{21} < 0$  (strong asymmetry).

Sampling  $10^5$  different instances for different  $\sigma$  and fixed  $\Delta h^c = 1$ , we look for a self-loop for any  $H$ , and represent the parameters leading to self-loops in the  $(c_{12}, c_{21})$ -plane (Figs. S8). In the limit of binary spins ( $\sigma = 0$ ), we recover the necessary and sufficient conditions for self-loops to emerge, i.e.  $c_{12}c_{21} < 0$  and  $|\Delta c| > |\Delta h^c|$  (Fig. S8-a). For

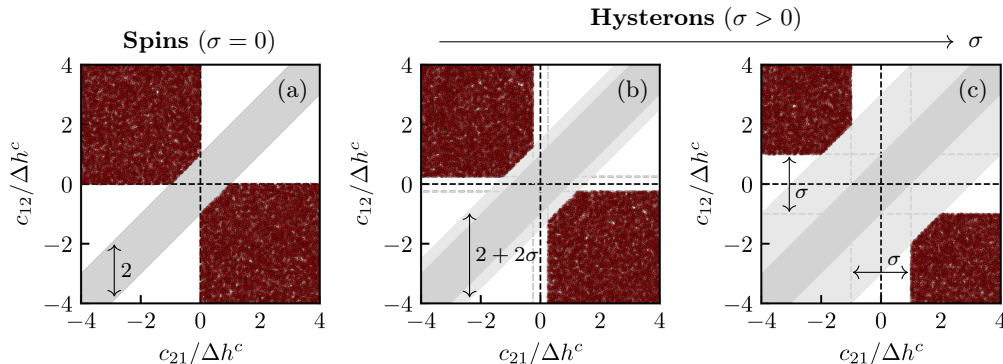


FIG. S8: **Sampling self-loops for  $N = 2$  interacting elements.** Self-loops of size 4 for arbitrary couplings in the  $(c_{12}, c_{21})$ -plane (red transparent markers); (a) spins, i.e.  $\sigma = 0$ ; (b-c) hysterons, for  $\sigma = 0.5$  (b) and  $\sigma = 2$  (c).

$\sigma > 0$ , numerical results are consistent with the conditions given by Eqs. (S16) (Figs. S8-b and c). We find similar results when the two hysterons' spans are different (not shown here).

Altogether, at the level of  $N = 2$  interacting elements, the microscopic hysteresis tends to prevent  $L = 4$  self-loops that would have been possible otherwise, but in all cases strong asymmetry is a necessary condition for self-loops to emerge.

### 8.3. Large systems

The sufficient and necessary conditions for  $L = 4$  self-loops to emerge in systems of  $N = 2$  spins can be extended into necessary conditions for  $L = 4$  self-loops to emerge for arbitrary  $N$ . Starting with spins and noting that each  $L = 4$  self-loop only involves two spins ( $k$  and  $l$ ), we find that such  $L = 4$  loop can only occur when  $c_{kl}c_{lk} < 0$  and  $|\Delta c_{kl}/\Delta \tilde{h}_{kl}^c| > 1$ , where  $\Delta c_{kl} = c_{kl} - c_{lk}$  and where

$$\tilde{h}_i^c = h_i^c - \sum_{j \neq k, l} c_{ij} s_j. \quad (\text{S17})$$

Hence, for arbitrary  $N$ , the effect of the  $N - 2$  spins that do not flip is to effectively rescale the difference between the switching fields of the two flipping spins. Therefore, the same way as for  $N = 2$ , self-loops of size  $L = 4$  only emerge for strong asymmetry ( $c_{kl}c_{lk} < 0$ ) and large enough asymmetry  $|\Delta c_{kl}|$ . However, in contrast with  $N = 2$ , when a pair of spins satisfies the conditions above (for a given configuration of the rest of the system), it does not imply that the system has a way to land on the cycle, as it might be disconnected from the stable states in phase space.

We confirm the results above by sampling  $10^5$  systems with  $N = 1024$  elements, and looking for self-loops at any  $H$ . We plot a red marker in the rescaled  $(c_{12}, c_{21})$ -plane when we find a  $L = 4$  self-loop, where 1 and 2 now represent the two flipping elements. We focus on the large coupling limit ( $NJ_0 = 10$ ), for collections of spins (Fig. S9-a) and hysterons (Fig. S9-b).

We first focus on the case of spins. When self-loops occur, we find they are necessary included in the region of the rescaled  $(c_{12}, c_{21})$ -plane where  $L = 4$  self-loops occur for  $N = 2$  spins. However, for some systems there exist pairs of spins which are in the *red* region (for a given configuration of the rest of the system), but which are never involved in a  $L = 4$  self-loop. The situation is very similar for hysterons with distributed spans: we find self-loops in the same region as for spins, though there are fewer self-loops, especially close to the boundaries.

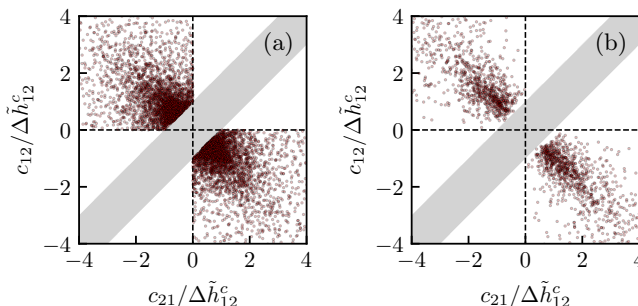


FIG. S9: **Self-loops of size 4 in large systems.**  $L = 4$  Self-loops for arbitrary couplings in the  $(c_{12} - c_{21})$  plane (red transparent markers); in the limit of binary spins (a), i.e.  $\sigma_i = 0$ , and for hysterons (b), i.e. with  $\sigma_i$  flatly sampled from  $[0, 0.5]$ ; fixed  $N = 1024$ , and  $NJ_0 = 10$ .

### 8.4. Preventing $L = 4$ self-loops

We note that the condition to prevent  $L = 4$  self-loops consists in a simple and a complex part, and we refer to the simple part -  $c_{ij}c_{ji} > 0$  for all pairs  $(i, j)$  - as the condition of weak asymmetry. This simple condition is sufficient to guarantee the absence of  $L = 4$  self-loops for any system size, although, as there are other parts in hysteron parameter space where such self-loops are prevented - it is overly restrictive.

## 9: Well-behaved coupling classes

In this section, we provide illustrations for the different classes of well-behaved models discussed in the main text.

### 9.1. Reciprocal couplings

Reciprocal couplings are reminiscent of dilute interacting soft spots, as discussed in [5]. Soft spots correspond to local rearrangements associated with quadrupolar Eshelby-like displacement fields (Fig. S10-a). In this context, the binary elements have all the same size, which implies  $c_{ij} = c_{ji}$ , and the sign of the interaction coefficient is given by their relative orientations. When compatible lobes of the fields face each other, the interaction is rather ferromagnetic ( $c_{ij} > 0$ ), while it is rather antiferromagnetic ( $c_{ij} < 0$ ) when incompatible lobes face each other.

### 9.2. Constant-columns couplings

Constant-columns couplings can be derived from mechanical equilibrium in a linear chain of mechanical hysterons (Fig. S10-b). The force-displacement curve of a mechanical hysteron is given by a bilinear relation:

$$f_i = u_i - d_i s_i, \quad (\text{S1})$$

with  $f_i$  the force,  $u_i$  the displacement,  $d_i$  the force discontinuity and  $s_i$  the state (Fig. S10-d). The mapping reads  $c_{ij} = -d_j$  with  $d_j > 0$ , where  $H = U = \sum_i u_i$  is the total displacement [12].

### 9.3. Ferromagnetic couplings

Ferromagnetic couplings can be derived from mechanical equilibrium in a parallel arrangement of mechanical hysterons in series with a spring of stiffness  $k$  [26] (Fig. S10-d). The mapping reads  $c_{ij} = d_j/k$  with  $d_j > 0$ , where  $H = U$  is the total displacement [26].

Note that a collection of hysterons arranged in parallel as represented in Fig. S10-c interact ferromagnetically, and the interaction matrix has the same structure as for constant-columns couplings: when a hysteron snaps, it affects

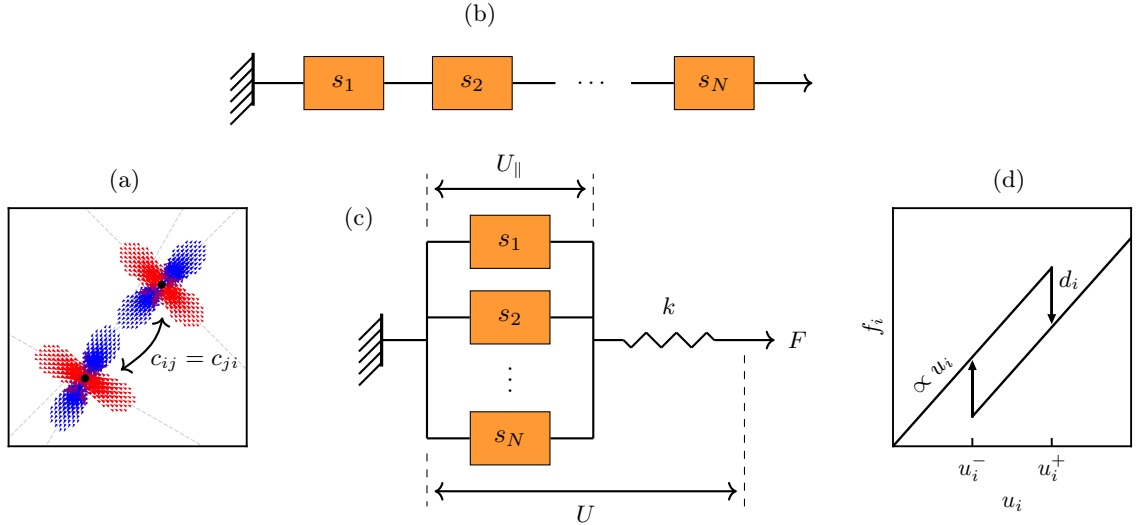


FIG. S10: **Realizations of the different interaction classes.** (a) Reciprocal couplings: two interacting soft spots, associated with quadrupolar displacement fields, interact reciprocally: blue arrows: inward displacements; red arrows: outward displacements. In this example, the orientations of the quadrupoles are such that  $c_{ij} = c_{ji} < 0$  due to the incompatibility of the quadrupolar fields. (b) Constant-columns couplings: linear chain of mechanical hysterons. (c) Parallel couplings: parallel arrangement of mechanical hysterons in series with a spring of stiffness  $k$  and zero-rest-length. (d) Force-displacement curve for a single mechanical hysteron.

the switching fields of all the other hysterons the same way. Remarkably, the spring in series plays a crucial role in allowing for the interaction by transmitting the force jumps through its deformation.

#### 9.4. Constant-rows couplings

The case of constant-rows couplings is relatively artificial as it corresponds to a case where hysterons are affected by the snap of the other hysterons exactly the same way, independently of the hysteron snapping. It is likely that this interaction matrix cannot be derived from mechanical equilibrium of mechanical hysterons, but it is an insightful example of well-behaved coupled hysterons model.

### 10: Role of the race condition rules

In this section, we analyze the impact of different race condition rules on the probability of finding self-loops and on the self-loop sizes distribution. We explore four different dynamical rules. Rule 0 considers the model ill-defined whenever race conditions occur [12, 21] (discarding the associated instance), but prevents sampling large systems (see section 2). Rule 1 (focus of the main text) and 1' specify to flip only the most and the least unstable element, respectively. Finally, under rule 2, all unstable elements are flipped simultaneously. Table SI summarizes the ill-defined cases encountered in each different classes of couplings for the different dynamical rules.

Coupling class	rule 0	rule 1	rule 1'	rule 2
Arbitrary	RC/G/SL	G/SL	G/SL	G/SL <sup>†</sup>
Reciprocal	RC	–	–	SL*
Constant-columns	RC	–	–	SL*
Constant-rows	RC	–	–	SL*
Ferromagnetic	RC	–	–	–

\*  $L = 2$  self-loops only. <sup>†</sup> All  $L \geq 2$  self-loops allowed.

Table SI: Summary of the different classes of coupled hysteron models. Ill-definition problems, for a given class of couplings and a given choice of race condition rule; RC: race conditions; G: gaps; SL: self-loops.

#### 10.1. Arbitrarily-coupled hysterons

Here, we focus on hysterons with random asymmetric couplings. First, in the case where all unstable hysterons flip simultaneously (rule 2), we find that all self-loop sizes are allowed starting from  $L = 2$  (Fig. S11-h). In contrast, all race conditions rules which involve flipping elements one by one (rules 0, 1, and 1') lead to self-loops whose sizes are always even, starting from 4 (Figs. S11-e to g). This is expected given all the hysterons involved in a self-loop must first snap and then unsnap, leading to the parity observed.

Let us show that self-loops of size  $L = 2$  are forbidden when hysterons flip one-by-one, because they correspond to loops involving a single hysteron with negative span. Let us consider that state  $S$  is unstable at a given value of the drive  $H$  because hysteron  $i$  is unstable, e.g.  $H > H_i^+(S)$  (without loss of generality). The system enters a self-loop of size 2 if hysteron  $i$  remains unstable after the snap, i.e.  $H < H_i^-(S)$ , which yields:

$$h_i^- - \sum_{j \neq i} c_{ij} s_j > h_i^+ - \sum_{j \neq i} c_{ij} s_j. \quad (\text{S1})$$

All hysterons  $j \neq i$  being unchanged, Eq. (S1) implies  $h_i^- > h_i^+$ , which corresponds to hysteron  $i$  having a negative span, i.e.  $\sigma_i < 0$ .

Interestingly, for all race condition rules, the probability of finding a self-loop increases as a power law for  $NJ_0 \ll 1$ , and saturates toward a constant value with  $J_0$  for  $NJ_0 \gg 1$  (Figs. S11-a to d). Except for rule 0, the large- $J_0$  plateau value increases monotonically with  $N$ , and in all cases the data suggests that  $P_{sl} \rightarrow 0$  when  $N$  increases. Moreover, in

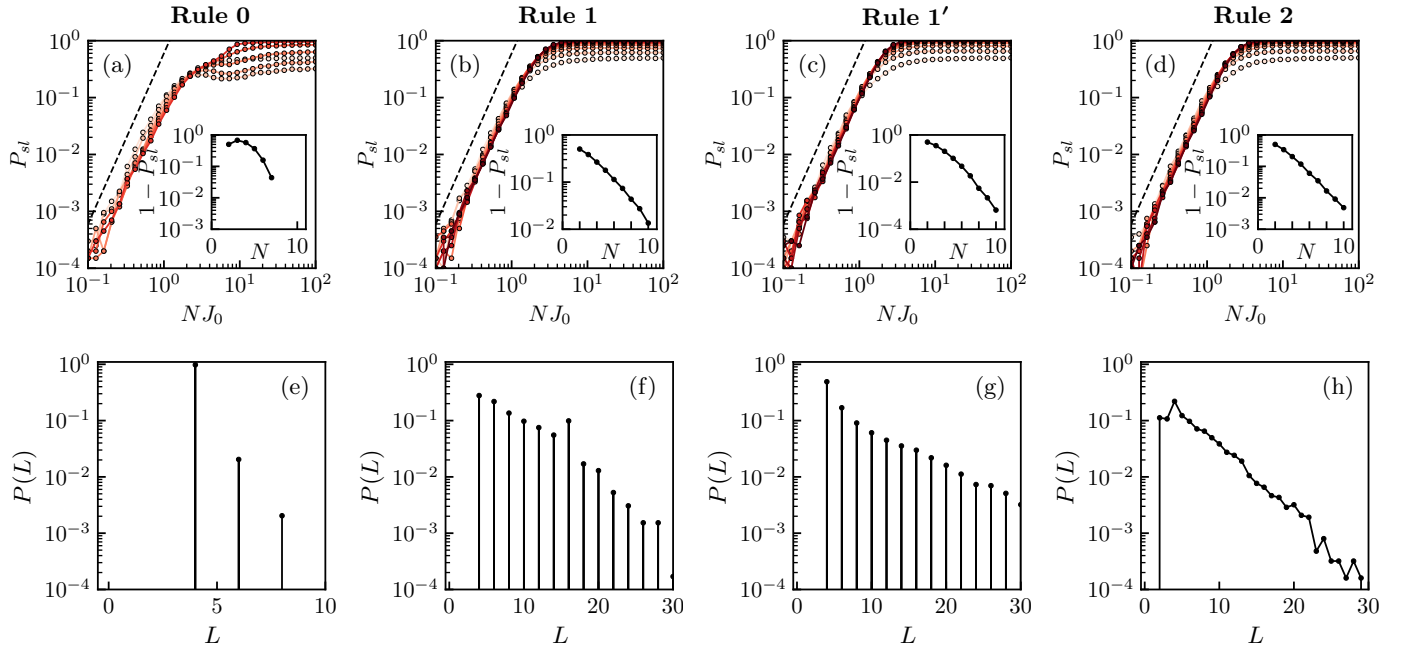


FIG. S11: **Self-loop statistics for arbitrarily-coupled hysterons and different race condition rules.** (a-d) Probability  $P_{sl}$  of at least one self-loops occurring for any  $H$  as a function of  $NJ_0$ , for different  $N \in [2, 3, \dots, 10]$ , color-coded from light to dark red as  $N$  increases; the black dashed lines represent the slope 3; (inset) probability to be self-loop free  $1 - P_{sl}$  as a function of  $N$  in the large coupling limit ( $NJ_0 = 10^2$ ). (e-h) Self-loops size distributions for fixed  $NJ_0 = 20$  and  $N = 8$ . (a/e) Rule 0; (b/f) rule 1; (c/g) rule 1'; (d/h) rule 2.

all cases, the size of self-loops seems to be exponentially distributed, modulo the specific constraints on the self-loop sizes discussed above.

## 10.2. Well-behaved models

Here, we focus on the well-behaved models introduced in the main text, namely reciprocal, constant-columns, and ferromagnetic couplings. We have shown that self-loops are forbidden for all these classes when hysterons flip one by one (rules 0, 1 and 1'). Here, we analyze the probability of finding self-loops and the self-loop size distributions when race conditions are resolved with rule 2.

Let us first focus on reciprocal, constant-columns, and constant-rows couplings. We find that all self-loops have size  $L = 2$ , independently of the model (not shown here). The presence of 2-cycles is a well-known feature for reciprocally-coupled spins where all unstable spins flip simultaneously [33, 34, 38], which is generally called synchronous or parallel update in the context of spin glasses and neural networks. Second, the probability  $P_{sl}$  of finding at least one  $L = 2$  self-loop for any  $H$  increases as a power law for  $NJ_0 \ll 1$ , and saturates toward a constant value with  $J_0$  for  $NJ_0 \gg 1$

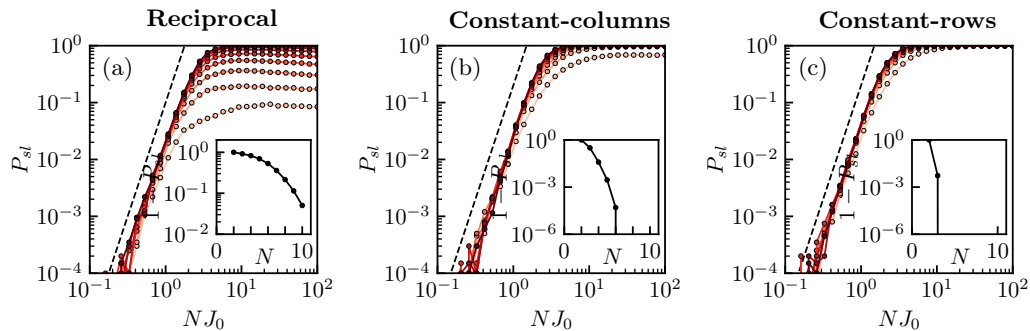


FIG. S12: **Self-loop statistics for well-behaved models of coupled hysterons**, where race conditions are resolved with rule 2. Statistical measures for self-loops scale when plotted as function of  $NJ_0$  and dominate for  $NJ_0 \gg 1$  ( $10^5$  samples; color from light to dark as  $N$  increases from 2 to 10). Probability  $P_{sl}$  of finding at least one self-loop for any value of  $H$  (dashed line indicates slope 4). Inset: The probability to be self-loop free,  $1 - P_{sl}$ , decays to zero with  $N$  for large couplings ( $NJ_0 = 10^2$ ). (a) Reciprocal couplings; (b) constant-columns couplings; (c) constant-rows couplings.

(Figs. S12), which asymptotes to 1 as  $N$  increases (Figs. S12-insets)

Finally, for purely ferromagnetic couplings, we find no self-loops when race conditions are resolved with rule 2. It suggests that the 2-cycles emerging with rule 2 are more related to the presence of antiferromagnetic interactions than to non-symmetric ones, which is very different than in the case where hysterons flip one by one.

## 11: Self-loop structures

Transition graphs (t-graphs) have emerged as a powerful framework for capturing and studying sequential responses [3, 18, 21, 31]. In these, states  $S$  are represented by nodes, and their transitions under zero-temperature, quasistatic driving with a global field  $H$  form directed edges (Fig. 1-c of the main text, and Figs. S16). The range of stability of state  $S$  is given by its upper and lower switching fields  $H^\pm(S)$  (which follow from the extrema of  $H_i^\pm(S)$ , see main text), and an up or down transition is initiated when  $H > H^+(S)$  or  $H < H^-(S)$ . Here, we use the framework of t-graph to represent the structures of the different possible self-loops. Therefore, we will restrict to only represent the unstable states involved in said self-loops.

### 11.1. Algorithm to generate different self-loop structures

The fundamental self-loops are those where  $n_e = N$  with an arbitrary labeling (see main text). To naively find all  $(n_e, L)$  fundamental self-loops, one needs to find all loops of length  $L$  starting from a corner of a  $n_e$ -hypercube, and then multiply by the number of states which is  $2^{n_e}$ . For example, for  $n_e = 3$ , there are 24 self-loops of length  $L = 6$  starting from the state  $S = (-1 - 1 - 1)$ . Multiplying by the number of states which is  $2^3 = 8$ , we find 192 self-loops. Among these self-loops, there are many duplicates. While we can filter these out manually, it is more efficient to write our algorithm such that it prevents generating duplicates by construction.

There are two factors to take into consideration which cause duplicates. The first issue is permutation symmetry. For example, the sequence of flips  $(2, 1, 0, 2, 0, 1)$  from state  $(+1 - 1 - 1)$  gives rise to the same self-loop as the sequence  $(1, 0, 2, 1, 2, 0)$  from state  $(-1 - 1 + 1)$ , except for an arbitrary permutation of the hysterons labeling (Fig. S13). We can break this permutation symmetry by indexing hysterons according to the order in which they are flipped. Using this convention, we find that only the first sequence  $(2, 1, 0, 2, 0, 1)$  from state  $(+1 - 1 - 1)$  has the proper labeling. This convention reduces the number of generated self-loops by a factor  $n_e!$ . Using this convention, for  $n_e = 3, L = 6$  we find four self-loops from  $(-1 - 1 - 1)$ . Multiplying this by the number of states, we find 32 loops in total.

The second issue is that any state in a self-loop can be the starting state. For example, the sequence  $(2, 1, 0, 2, 0, 1)$  from state  $(+1 - 1 - 1)$  can also be 'shifted' by one, such that we obtain the sequence  $(1, 0, 2, 0, 1, 2)$  from state  $(+1 - 1 + 1)$ ; with the labeling convention described above, this becomes  $(2, 1, 0, 1, 2, 0)$  from state  $(+1 + 1 - 1)$  (Fig. S14). We can partially solve this issue by breaking up the self-loops by the minimum magnetisation of the states they visit:

$$M(n_e, L) = \sum_{m=-n_e}^{n_e} M_m(n_e, L) \quad (\text{S1})$$

where  $M_m(n_e, L)$  is the number of  $(n_e, L)$  self-loops which starts and ends at the same magnetisation  $m = \sum_i s_i$ , and does not go below  $m$ . This convention filters out loops such as  $(2, 1, 0, 1, 2, 0)$  from state  $(+1 + 1 - 1)$ . For  $n_e = 3, L = 6$ , this reduces the number of self-loops from 32 to 7.

These two conventions prevent most duplicates, but not all: we have taken care of shifts to states with a different magnetization from the initial state, but this still leaves shifts to states with the *same* magnetization as the initial state. For our example, the loop  $(2, 1, 0, 2, 0, 1)$  from state  $(+1 - 1 - 1)$  can be shifted by four to obtain the transition

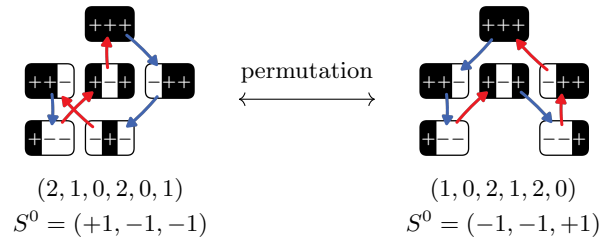


FIG. S13: **Permutation symmetry between two self-loops.** Each self-loop is defined by the sequence of flips and the starting state  $S^0$ . Two self-loops are the same if one can be obtained from the other by a permutation of the hysterons labeling.



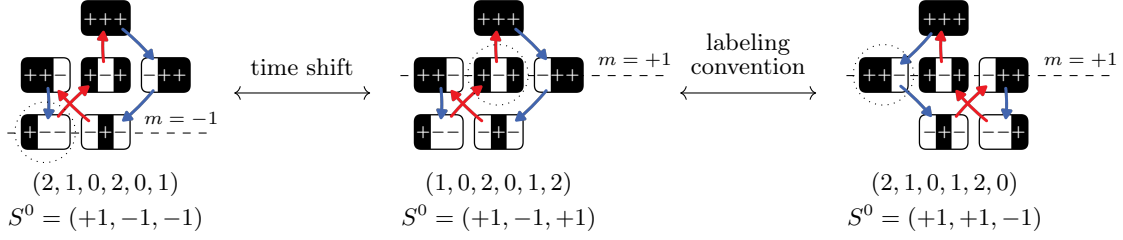


FIG. S14: **Time shift symmetry between two self-loops.** Each self-loop is defined by the sequence of flips and the starting state  $S^0$ . Two self-loops are the same if one can be obtained from the other by arbitrarily shifting the starting state. This ambiguity on the starting state is partially lifted by decomposing self-loops by the magnetization  $m$  of their starting state, and imposing the magnetization cannot go below  $m$ .

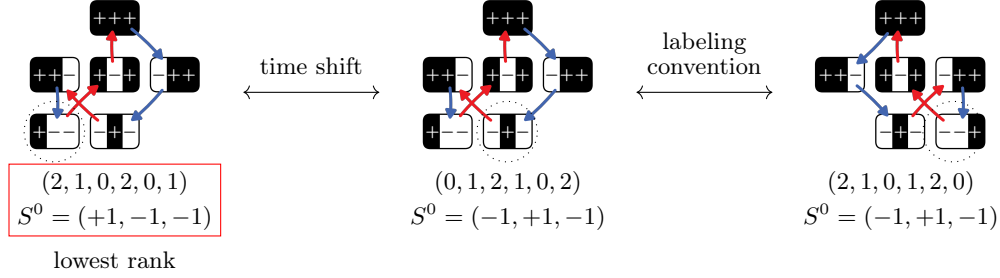


FIG. S15: **Time shift symmetry between two self-loops.** To remove the final ambiguity on the starting state when there exist multiple possible starting states with the same magnetization, we compare the ranking of self-loops (see text), and pick the loop with the smallest ranking.

sequence  $(2, 1, 0, 1, 2, 0)$  from state  $(-1 + 1 - 1)$  (Fig. S15). To deal with this issue, we assign to each of these loops a ranking composed of their initial state and the sequence of flipped hysterons: in the above example these rankings would be  $100210102$  and  $010210120$  (replacing all the phases  $-1$  by  $0$ ). We only count the loop which has the lowest ranking – note that the rankings are only the same if the loops are exactly the same. This method allows us to identify one more pair of duplicates for  $n_e = 3, L = 6$  – namely, the two loops described above – bringing the final number of ( $n_e = 3, L = 6$ ) fundamental self-loops down to 6, as shown in the main text.

The results are summarized in Table SII and Fig. S16, and emphasize the proliferation of the number of self-loop

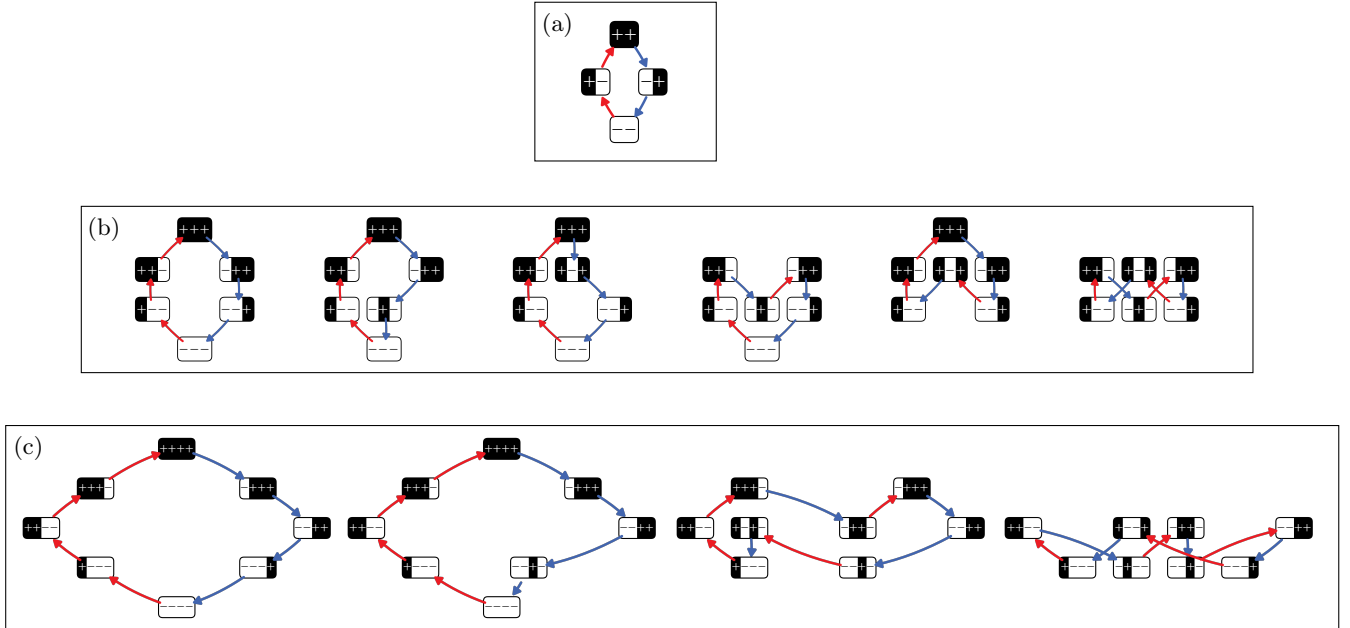


FIG. S16: **Ensembles of self-loops of different sizes.** Blue(/red) arrows represent up(/down) transitions;  $+1/-1$  are represented with full/empty circles. By convention, the elements are indexed according to their up sequence starting from the lower saturating state. (a) Size  $L = 4$  (1 self-loop). (b) Size  $L = 6$  (6 self-loops). (c) Size  $L = 8$  (58 self-loops, not all shown).

	$n_e = 2$	$n_e = 3$	$n_e = 4$	$n_e = 5$
$L = 4$	1	–	–	–
$L = 6$	–	6	–	–
$L = 8$	–	2	56	–
$L = 10$	–	–	176	796
$L = 12$	–	–	420	9028
$L = 14$	–	–	448	76640
$L = 16$	–	–	112	535584
$L = 18$	–	–	–	x
$L = 20$	–	–	–	x
$L = 22$	–	–	–	x
$L = 24$	–	–	–	x
$L = 26$	–	–	–	x
$L = 28$	–	–	–	x
$L = 30$	–	–	–	x
$L = 32$	–	–	–	15109096

Table SII: **Number of self-loop structures which can be drawn.** The left column (resp. top row) indicates the size  $L$  of self-loops (resp. the number of hysterons involved in the loop  $n_e$ ); the number inside each box is the number of different self-loop structures that can be drawn (not all of them are realizable with pairwise interactions).

	$n_e = 2$	$n_e = 3$	$n_e = 4$	$n_e = 5$
$L = 4$	1	–	–	–
$L = 6$	–	6	–	–
$L = 8$	–	0	56	–
$L = 10$	–	–	114	796
$L = 12$	–	–	145	x
$L = 14$	–	–	48	x
$L = 16$	–	–	4	x
$L = 18$	–	–	–	x
$L = 20$	–	–	–	x
$L = 22$	–	–	–	x
$L = 24$	–	–	–	x
$L = 26$	–	–	–	x
$L = 28$	–	–	–	x
$L = 30$	–	–	–	x
$L = 32$	–	–	–	x

	$n_e = 2$	$n_e = 3$	$n_e = 4$	$n_e = 5$
$L = 4$	0	–	–	–
$L = 6$	–	2	–	–
$L = 8$	–	0	24	–
$L = 10$	–	–	4	376
$L = 12$	–	–	1	x
$L = 14$	–	–	0	x
$L = 16$	–	–	0	x
$L = 18$	–	–	–	x
$L = 20$	–	–	–	x
$L = 22$	–	–	–	x
$L = 24$	–	–	–	x
$L = 26$	–	–	–	x
$L = 28$	–	–	–	x
$L = 30$	–	–	–	x
$L = 32$	–	–	–	x

Table SIII: **Number of self-loop structures which are realizable.** The left column (resp. top row) indicates the size  $L$  of self-loops (resp. the number of hysterons involved in the loop  $n_e$ ); the number inside each box is the number of different self-loop structures which are realizable (left), and which are realizable when restricting to weak asymmetry (right).

structures when  $L$  and  $n_e$  increase.

### 11.2. Realizability of self-loops

Now that we have established the different possible self-loop structures for a given pair  $(n_e, L)$ , we can in principle determine the necessary conditions to prevent any self-loop. For every self-loops structure, it is indeed possible to find a set of linear inequalities of the hysteron parameters  $h_i^\pm$  and  $c_{ij}$  [21, 30, 31] which is associated to the emergence of said self-loop. This is done using linear programming and a variation on the methods introduced in [31]. We make three changes with respect to the previously introduced framework: these concern the self-loops themselves, the critical driving that initiates a transition, and the rule which we use to deal with race conditions.

While the framework in [31] did not explicitly discuss conditions to realize self-loops, these conditions follow naturally from the techniques described. Namely, for a non-loop transition of length  $L$ , the conditions are split between the initial state  $S^0$ , the final state  $S^L$ , and a number of intermediate states  $S^1, \dots, S^{L-1}$ . In the case of a self-loop, there is no final state  $S^L$ , as the transition instead returns to its initial state  $S^0$ . Consequently, to realize a self-loop from a given state  $S^0$ , it suffices to only construct the initial and intermediate inequalities for the states  $S^0, S^1, \dots, S^{L-1}$ .

A second divergence from the framework in [31] is that we are not interested in whether a self-loop arises for a specific driving  $H$ . While the previous framework assumes that  $H = H^\pm(S^0)$ , for our purposes it is sufficient if a self-loop is realizable for *any* driving. We account for this by eliminating the driving from the set of linear inequalities. For example, if we have the set of inequalities

$$\begin{aligned}
 H &> H^+(S^0), \\
 H &< H^-(S^1), \\
 H &> H^+(S^2), \\
 H &< H^-(S^3), \\
 H &> H^+(S^4), \\
 H &< H^-(S^5),
 \end{aligned} \tag{S2}$$

which realizes a self-loop of length  $L = 6$ , we can eliminate the driving  $H$  to obtain:

$$\begin{aligned}
 H^-(S^1) &> H^+(S^0), \\
 H^-(S^1) &> H^+(S^2), \\
 H^-(S^1) &> H^+(S^4), \\
 H^-(S^3) &> H^+(S^0), \\
 H^-(S^3) &> H^+(S^2), \\
 H^-(S^3) &> H^+(S^4), \\
 H^-(S^5) &> H^+(S^0), \\
 H^-(S^5) &> H^+(S^2), \\
 H^-(S^5) &> H^+(S^4).
 \end{aligned} \tag{S3}$$

Essentially, this set of inequalities enforces that there is a range of the driving  $H$  where a self-loop occurs.

A final complication arises from the rule that we use to resolve race conditions, which were considered ill-defined in [31]. The application of this rule loosens the requirements for a given self-loop: whereas the hysteron that flips for each step of the transition previously needed to be the *only* unstable hysteron, now it merely needs to be the *most* unstable. A great benefit of this rule is that we do not need to keep track of the full range of switching fields  $H_i^\pm(S)$ , but only of the state switching fields  $H^\pm(S)$ .

An edge case occurs, however, for states that are 'unconditionally unstable' – i.e.,  $H^-(S) > H^+(S)$ . While these states pose no issue if  $H > H^+(S)$  or  $H < H^-(S)$ , the range  $H^-(S) < H < H^+(S)$  is problematic, as in this case one cannot judge whether a hysteron flips up or down from the ordering of the switching fields alone. As a proper accounting for these cases would significantly increase the complexity of the inequalities, we choose to take a more conservative approach, where a self-loop is counted as non-realizable if it is contingent upon this edge case.

The results of our realizability checks are shown in Tables SIII, for the general case (left), and in the case of weak asymmetry (right).

## 12: Response of well-behaved models

The absence of self-loops in the different well-behaved models allows to explore statistics of avalanches and of the response to cyclic drive for large  $N$  and arbitrary  $J_0$ . We focus below on race condition rule 1, where the most unstable element flips first, and on ensembles of hysterons with distributed spans ( $\sigma_i$  flatly sampled from  $[0, 0.5]$ ).

### 12.1. Avalanche sizes

We consider  $N = 1024$  hysterons and place ourselves at  $H = 0$ . Starting from a random initial condition, the system is stabilized by flipping unstable hysterons one by one until a stable state  $S^0$  is found (which is guaranteed in the absence of self-loops). We simulate  $S^0 \rightarrow S^1$  over  $5 \times 10^3$  samples, and record avalanche sizes  $A$  – the number of elements flips before the system settles on a stable state. For all models, when  $NJ_0 \ll 1$ , only Preisach-like non-avalanche transitions ( $A = 1$ ) are found. For reciprocal couplings, the larger  $J_0$ , the broader the avalanche size distribution and the larger the mean avalanche size, with a transition around  $NJ_0 \simeq 1$  (Figs. S17-a and b). For  $NJ_0 \gg 1$ , avalanche sizes are power-law distributed with a cutoff growing with  $J_0$  and  $N$ , and saturating below system size. For constant-columns couplings, we find a similar transition scenario at  $NJ_0 \simeq 1$  (Figs. S17-c and d). However, for  $J_0 \simeq 1$ , the mean avalanche size reaches a maximum increasing with system size (Fig. S17-d, inset), then decreases abruptly, and increases again for larger  $J_0$ . Finally, for constant-rows couplings, numerical simulations confirm that transitions can only be Preisach-like nonavalanche transitions or horizontal avalanches of size 2 (Figs. S17-e and f), with a transition between the two around  $NJ_0 \simeq 1$ .

### 12.2. Response to cyclic drive

Let us now consider cyclic drive conditions - when the input  $U$  is swept between  $U_{\min}$  and  $U_{\max}$ . We focus on two aspects of the response: the number of driving cycles  $\tau$  taken to reach a periodic orbit, and the period  $T$  of the orbit relative to the driving cycle. In the Preisach model (limit of zero couplings),  $\tau \leq 1$  and  $T = 1$ , which can be understood by noting that each (independent) hysteron requires at most one cycle before it reaches a periodic orbit. Only a few results exist for finite interactions between hysterons. For small systems, it was shown that the transients  $\tau$  and periodicity  $T$  are distributed exponentially [4].

Here, we consider  $N = 512$  hysterons and place ourselves at  $U = 0$ . Starting from a random initial condition,

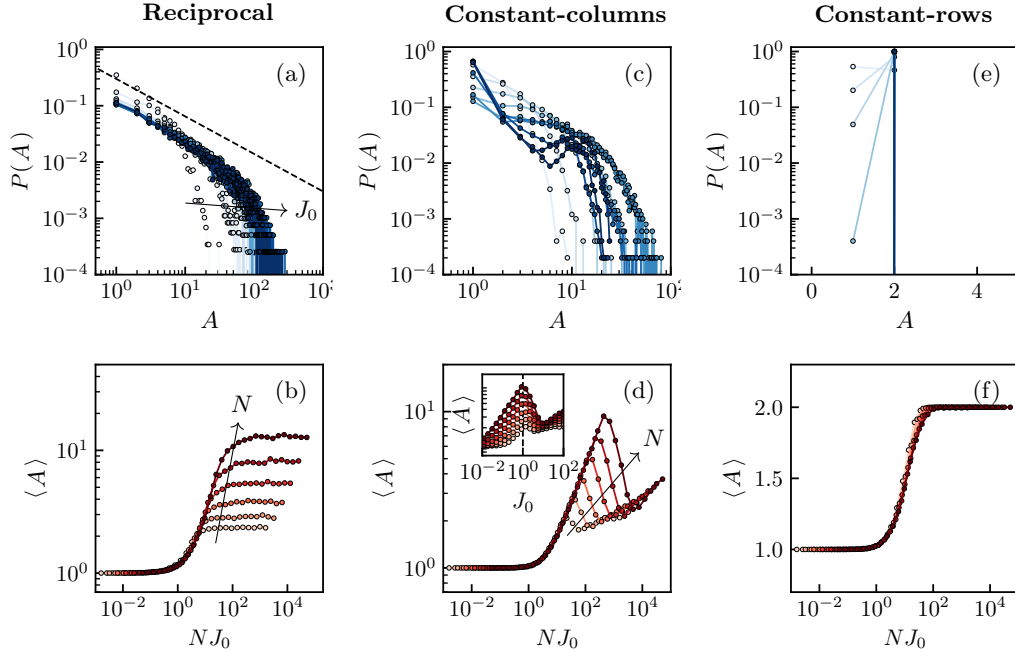


FIG. S17: **Large avalanches for well-behaved models**, where race conditions are resolved with rule 1. (a/c/e) Avalanche size distributions for different  $J_0 \in [10^{-2}, 10^2]$ ; color-coded from light to dark blue as  $J_0$  increases; fixed  $N = 1024$ . (b/d/f) Mean avalanche size  $\langle A \rangle$  as a function of  $NJ_0$ , for different  $N \in [16, 32, 64, 128, 256, 512]$ , color-coded from light to dark red as  $N$  increases. (left) Reciprocal couplings; (middle) constant-columns couplings; (right) constant-rows couplings.

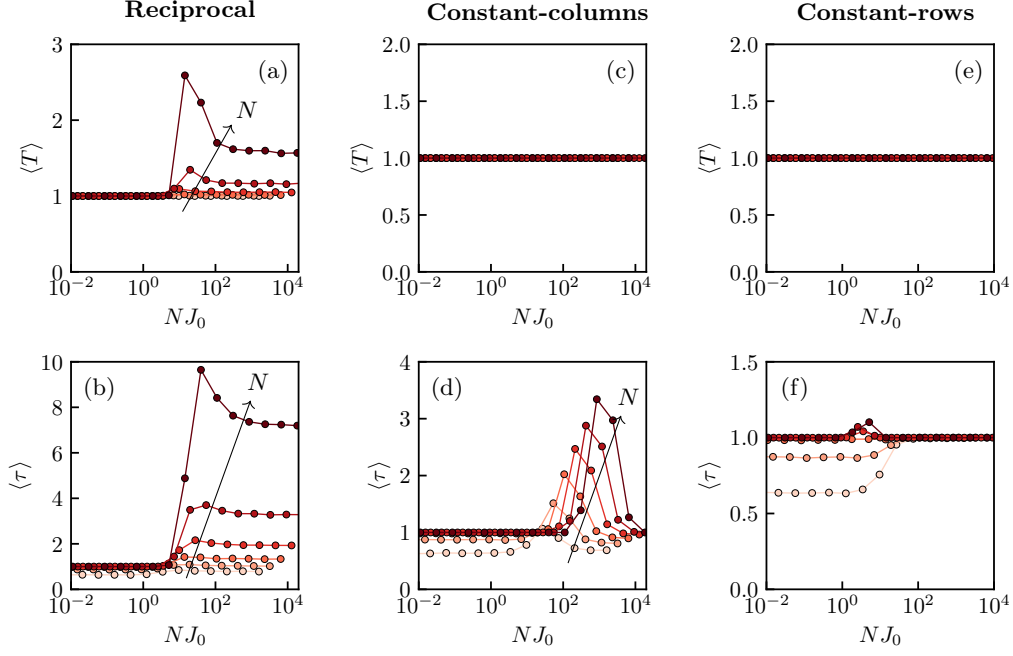


FIG. S18: **Transients and periodicity during cyclic drive for the well-behaved models**, where race conditions are resolved with rule 1, for different  $N \in [16, 32, 64, 128, 256, 512]$ , color coded from light to dark red as  $N$  increases. (a/c/e) Ensemble averaged transient length  $\langle \tau \rangle$  as a function of  $J_0$ . (b/d/f) Ensemble averaged periodicity  $\langle T \rangle$  as a function of  $J_0$ . (left) Reciprocal couplings; (middle) constant-columns couplings; (right) constant-rows couplings.

the system is stabilized by flipping unstable hysterons one by one until a stable state is found. Finally, the drive  $U$  is swept between 0 and  $U_{\max}$ , where  $U_{\max}$  is the drive amplitude leading to a magnetization  $m = \sum_i s_i/N$  equal or larger than 0.5 ( $U_{\max}$  is determined during the first drive cycle and is kept fixed for the rest of the simulation). For the reciprocally-coupled case (Figs. S18-a and b), when  $NJ_0 \ll 1$ , both  $\langle \tau \rangle$  and  $\langle T \rangle$  are equal to 1, and when  $NJ_0 \gg 1$ , both  $\langle \tau \rangle$  and  $\langle T \rangle$  are greater than 1 and constant with  $J_0$ . Remarkably, both  $\langle \tau \rangle$  and  $\langle T \rangle$  reach a maximum for intermediate  $J_0 \simeq 1/N$ . For constant-columns and constant-rows couplings, we systematically find  $T = 1$  (Figs. S18-c and e): all orbits have the same period as the drive. This is expected for constant-columns couplings given the absence of scrambling [12]. Also,  $\langle \tau \rangle = 1$  for both  $NJ_0 \ll 1$  and  $NJ_0 \gg 1$  (Figs. S18-c and e). For constant-columns couplings,  $\langle \tau \rangle$  reaches a maximum for intermediate  $J_0$  at the same value corresponding to the maximum of  $\langle A \rangle$ , i.e.  $J_0 \simeq 1$ . In contrast, for constant-rows couplings, the maximum of  $\langle \tau \rangle$  is reached for  $J_0 \simeq 1/N$ .